INVITED ARTICLE

PCCP
www.rsc.org/pccp

Conical intersections: A perspective on the computation of spectroscopic Jahn–Teller parameters and the degenerate 'intersection space'

Martin J. Paterson,[a] Michael J. Bearpark,[b] Michael A. Robb,*[b] Lluís Blancafort[c] and Graham A. Worth[d]

[a] *Department of Chemistry, University of Århus, DK-8000 Århus C, Denmark*
[b] *Department of Chemistry, Imperial College London, London, UK SW7 2AZ. E-mail: mike.robb@imperial.ac.uk*
[c] *Institut de Química Computacional, Departament de Química, Universitat de Girona, Campus de Montilivi, 17071 Girona, Spain*
[d] *School of Chemistry, University of Birmingham, Birmingham, UK B15 2TT*

Received 28th October 2004, Accepted 15th March 2005
First published as an Advance Article on the web 7th April 2005

We present a perspective on the computation and interpretation of force constants at points of symmetry-induced (Jahn–Teller) conical intersection. Our method is based upon the projection of the 'branching space' from the full $(3N - 6)$-dimensional Hessian for each component of a degenerate electronic state. For Jahn–Teller active molecules, this has the effect of removing the linear Jahn–Teller coupling from all but the interstate coupling and gradient difference vectors. The quadratic coupling constants are determined by the splitting of the harmonic vibrational frequencies within degenerate vibrational normal coordinates of the 'intersection space'. The potential energy surface topology along these normal modes is analogous to the Renner–Teller effect occurring in orbitally degenerate linear molecules. Our methodology gives a straightforward theoretical analysis of the various Jahn–Teller intersections and allows the determination of the seam curvature. Thus, we are in a position to compute the various Jahn–Teller coupling constants, in a particular coordinate system, and in addition to determine the nature of the high-symmetry Jahn–Teller geometry (*i.e.*, minimum or saddle-point on the seam). We illustrate these concepts with various examples of different Jahn–Teller conical intersections in some small molecules.

Introduction

Time-resolved laser spectroscopy is now commonly used to study the dynamics of ultrafast (<1 ps) photochemical processes.[1–8] Conical intersections between ground and excited state potential energy surfaces have proved to be essential for explaining the timescales and product distributions of these processes.[9–11] The role of conical intersections in photochemical reactions is difficult to probe directly by experiment, but is now well established computationally.[12–22]

There is, however, a type of conical intersection for which there is a long history of direct high-resolution spectroscopic work: the symmetry-induced crossings that occur in Jahn–Teller active molecules.[23–29] Commonly used spectroscopic techniques include photoelectron spectroscopy from a neutral closed-shell species to an open-shell Jahn–Teller active species,[8,25,30–34] and laser-induced fluorescence from a non-degenerate excited state to a degenerate state.[24,26,27,29,35–40] Here, measured vibronic energy levels can be compared directly with those calculated from parameterised model Hamiltonians, although there remain problems with the choice of Hamiltonian and calculating the necessary parameters.

The main purpose of this perspective article is to emphasise the connections between the study of photochemical processes and the spectroscopy of Jahn–Teller molecules. We have recently implemented a method for characterizing the conical intersection seam in terms of a quadratic expansion in curvilinear co-ordinates.[41] This offers a way to parameterise model Hamiltonians for spectroscopy, and to benchmark the computational methods used for locating intersections. However, we also develop this idea conceptually, to show that established ideas from Jahn–Teller theory offer a new perspective on the crossing seam for photochemical processes, where symmetry may not be involved. Recent calculations and experiments show that for photochemistry, decay away from the minimum energy point of a crossing may dominate,[14,42] in which case a systematic way of mapping out segments of the crossing seam will be invaluable.[16,41]

It is 75 years since von Neumann and Wigner[43] first discussed the existence of conical intersections between potential energy surfaces in polyatomic molecules. This was based upon a detailed analysis of the spectral representation of a symmetric (Hermitian) matrix and yielded the von Neumann–Wigner theorem, which states that in general two real parameters (three in the Hermitian case) need to be independently varied in order to achieve an eigenvalue degeneracy (see ref. 44 for a translation of the original article and ref. 45 for detailed discussion). Eight years later, Jahn and Teller proved in their seminal paper[46] that a polyatomic molecule in an orbitally degenerate electronic state is unstable with respect to linear displacement along some non-totally symmetric coordinates. The Jahn–Teller theorem[47,48] states that a molecule in an orbitally degenerate electronic state will distort along some non-totally symmetric vibrational coordinate which is determined by the symmetric square of the direct product of the degenerate irreducible representation (irrep) of the electronic state with itself. The Jahn–Teller theorem thus showed that for a polyatomic molecule belonging to a non-Abelian point group, the two degrees of freedom lifting the degeneracy transform as some non-totally symmetric irrep and will thus

DOI: 10.1039/b416538a

lower the symmetry. Jahn and Teller proved, by exhaustively looking at all possible molecular point groups, that these non-totally symmetric vibrations always exist; therefore there will always be modes of vibration which lift the degeneracy and lower the symmetry. The Jahn–Teller geometry is a conical intersection between the two components of the degenerate electronic state.

In non-cubic point groups, group theoretical analysis of Jahn–Teller degeneracies leads to a classification into E $\otimes$ e and E $\otimes$ ($b_1 \oplus b_2$) cases.[47–50] The former occurs in all point groups not containing a principal C_4 axis of symmetry, whereas the latter occurs when this is the case.[51] The nomenclature above indicates that a degenerate electronic state transforming as an E-type irreducible representation (irrep) interacts with a degenerate vibration, again transforming as an e-type irrep; or that a degenerate electronic state transforming as an E-type irrep interacts with two non-degenerate vibrations which transform as b_1 and b_2 irreps of the point group. The symmetries of the vibrations that lift the degeneracy can always be chosen to transform as a totally-symmetric and a non-totally symmetric irrep of an Abelian subgroup (*i.e.*, one containing no degenerate irreducible representations).

Any geometry of a molecule at which the electronic state is degenerate lies on a conical intersection seam between the potential energy surfaces of the components of the degenerate electronic state. Conical intersections can occur between electronic potential energy surfaces in Abelian point groups[50] (*e.g.*, an intersection between A_1 and B_2 electronic states in C_{2v} symmetry), and when there is no symmetry[52,53] (nominally C_1 point-group). These so-called accidental intersections are not required by symmetry, as in the Jahn–Teller case, but occur rather due to the nature of the two electronic states involved.

Conical intersections have been shown to be of considerable importance in organic[13–16,21,22] and inorganic[19,20] photochemistry in recent years. Points of intersection represent funnels for radiationless decay in polyatomic molecules.[9] This was first pointed out by Teller[54,55] as early as 1937, but it is only in the last decade that conical intersections have been routinely optimized.[56–58]

There are two vectors that lift the degeneracy linearly (*i.e.*, to first-order) at a conical intersection *via* the von Neumann–Wigner theorem.[43,59] These vectors define the 'branching space'.[60] The vectors spanning the 'branching space' are the gradient difference ($\boldsymbol{x}_1$) and interstate coupling vectors ($\boldsymbol{x}_2$).

$$\boldsymbol{x}_1 = \frac{\partial(E_2 - E_1)}{\partial \boldsymbol{\xi}} \tag{1}$$

$$\boldsymbol{x}_2 = \langle \boldsymbol{C}_2^t | \frac{\partial \hat{H}_e}{\partial \boldsymbol{\xi}} | \boldsymbol{C}_1 \rangle \tag{2}$$

where $\boldsymbol{\xi}$ is a vector of Cartesian displacements of the nuclei, $\hat{H}_e$ is the clamped nucleus electronic Hamiltonian operator, and $\boldsymbol{C}_i$ are the eigenvectors in a configuration interaction problem. It can be shown that the interstate coupling vector is parallel to the non-adiabatic coupling vector.[57] The degeneracy persists for an infinitesimal step in the orthogonal complement to the 'branching space': the 'intersection space'. However, the degeneracy can be lifted quadratically (*i.e.*, to second-order) by a finite step in this 'intersection space', in a manner analogous to the Renner–Teller effect[61–63] in orbitally-degenerate linear molecules (see Fig. 1).

A general conical intersection is found by simultaneously optimising the adiabatic energy gap and the projection of the upper state gradient onto the 'branching space'.[57] The 'branching space', also known as the $\boldsymbol{g}$–$\boldsymbol{h}$ plane,[45,52,53] forms the basis for locating and characterising a conical intersection geometry.[56,57] The location of low-energy domains of seams of intersection is now commonplace, and such regions represent key mechanistic elements in photochemical reaction modelling.[19–21] Until very recently however, the 'intersection space' has hardly been considered beyond the fact that it is the orthogonal complement to the 'branching space'. Yarkony[64] has noted that second-order terms become dominant in particular cases where one of the first-order terms has zero length. However, here we show, with several examples, that the second-order effects are important even if the first-order terms are not zero.

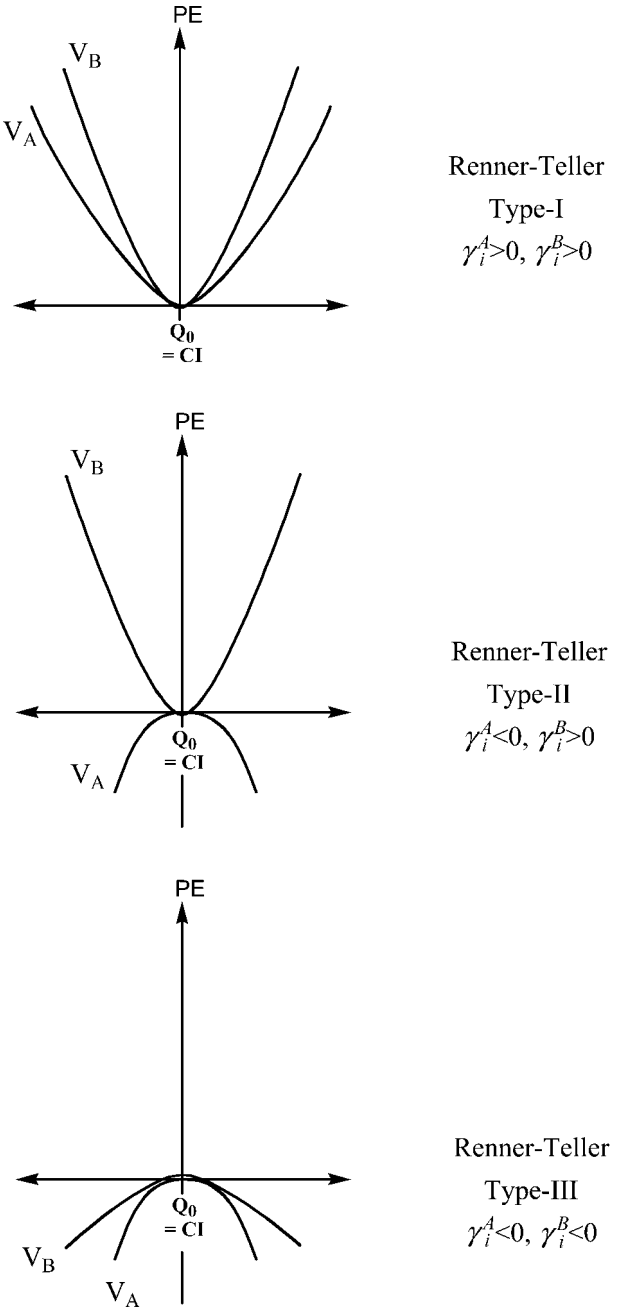

Fig. 1 Renner–Teller surface topologies.

The first point to make clear is that the degeneracy at a conical intersection is in fact lifted at second-order in any rectilinear coordinate system. This can be observed by analysing the 'intersection space' vibrational frequencies. To rationalise why the second-order effects are obtained in this way, one must recognise that the Hessian (force constants) for each state (*i.e.*, each component of the degenerate state at the intersection) is different. For the symmetry-imposed cases discussed in the present article, the frequencies and modes swap in degenerate pairs. In this respect, the well-known idea of quadratic Jahn–Teller coupling[23,24,26–28,47–49] is equivalent to second-order degeneracy lifting.

We shall now discuss the extended seam of intersection, which is a $(3N-8)$-dimensional hypercurve. We have recently shown how to calculate the curvature at a critical point on the seam using the first- and second-order potential constants.[41] Both first- and second-order effects contribute to the curvature of the seam and therefore it is important that we think beyond the 'branching space' and consider the 'intersection space' as well. The Jahn–Teller effect provides us with an excellent means of understanding both of these spaces since symmetry can be used. In addition, a more general understanding of the seam provides some new ideas about the Jahn–Teller effect itself. For example, for the cyclopropenyl radical we show that the higher symmetry D_{3h} Jahn–Teller point is in fact a saddle-point on the seam: there are lower energy critical points on the seam of both C_{3v} and C_s symmetry. Thus, although the degeneracy at the D_{3h} geometry is lifted at first-order as the Jahn–Teller theorem predicts, the seam in fact extends to lower symmetry structures. We can understand this once we recognize that the seam is a curvilinear combination of the first-order 'branching space' and the second-order 'intersection space'.

We begin with a brief discussion of the standard quadratic Jahn–Teller vibronic Hamiltonian and how it may be generalized. Notice that in the standard approach to Jahn–Teller systems, which can be termed the multi-mode approach,[50] all vibrations with the correct symmetry lift the degeneracy to first-order. In the model developed in this paper, which is formally equivalent, only two modes lift the degeneracy, but these coordinates change along the $(3N-8)$-dimensional seam. We then discuss the Renner–Teller effect in HCCS to highlight some pertinent facts about second-order degeneracy lifting. We follow this with a detailed discussion of the seam of intersection in the cyclopropenyl radical. We also discuss a simulation of the photoelectron spectrum of cyclobutadiene, where qualitative agreement between theory and experiment is possible using only a very minimal linear vibronic coupling model and wavepacket propagation techniques. Finally we compute the Jahn–Teller coupling constants for the cyclopentadienyl radical (Cp) in its $^2E_1''$ ground state. The quadratic coupling constants are computed to be quite small, in agreement with recent experimental studies.

The quadratic Jahn–Teller vibronic Hamiltonian

In this section we shall discuss the Hamiltonian used in spectroscopic studies of Jahn–Teller systems in more detail. In particular, we will focus on the ways in which symmetry can be used to simplify the expression. The quadratic form of the potential in this Hamiltonian can be written as a 2×2 matrix (labelled by the components of the degenerate electronic state), which is diagonalised to yield the potential energy surfaces.[50,65] The parameters of the quadratic form are referred to as coupling constants.[23,26–28] Once the potential constants are known from say theoretical computations, the full nuclear Hamiltonian, which can be represented in some suitable set of nuclear basis functions, *e.g.*, harmonic oscillator functions (Hermite polynomials), can be solved to give the vibronic energy levels for direct comparison with experiment. In practice this can only be performed for small systems, or with a reduced dimensionality.

In our theoretical development, we will discuss the form of the potential matrix for a general set of vibrational coordinates (Q_i). An example of such a set comes from the theoretical computation of photoelectron spectra,[50,66–68] where the neutral ground-state vibrational coordinate basis is used. This has the disadvantage that the interstate coupling and gradient difference vectors are not parallel to any normal modes of the appropriate symmetry. Rather they are linear combinations of the symmetry adapted normal modes for the ground state. This vibrational coordinate basis is generally used when fitting surfaces from single-point energy computations.

We develop an alternative set of coordinates ($\bar{Q}_i$) based upon the gradient difference vector and the interstate coupling vector, plus a set of $3N-8$ normal modes of the 'intersection space'. The latter set of coordinates has the advantage that all of the terms lifting the degeneracy at first-order are contained within the 'branching space'. Although in general the 'branching space' vectors are only defined to within a unitary transformation of each other, for the symmetric Jahn–Teller systems discussed below the vectors are uniquely defined through the largest Abelian subgroup.

We begin with a general discussion. The (non-relativistic) molecular Hamiltonian is,

$$\hat{H} = \hat{T}_N + \boldsymbol{V} \tag{3}$$

where $\hat{T}_N$ is the nuclear kinetic energy operator and $\boldsymbol{V}$ is the potential energy for the coupled electronic states. The potential matrix ($\boldsymbol{V}$) expanded to second-order around a point on a conical intersection seam in a set of general vibrational coordinates is given by,

$$\begin{aligned}\boldsymbol{V} = &\begin{pmatrix} \frac{1}{2}\sum_i^{3N-6} \omega_i Q_i^2 & 0 \\ 0 & \frac{1}{2}\sum_i^{3N-6} \omega_i Q_i^2 \end{pmatrix} \\ &+ \begin{pmatrix} \sum_i^{3N-6} \kappa_i^{A} Q_i & \sum_i^{3N-6} \kappa_i^{AB} Q_i \\ \sum_i^{3N-6} \kappa_i^{AB} Q_i & \sum_i^{3N-6} \kappa_i^{B} Q_i \end{pmatrix} \\ &+ \begin{pmatrix} \sum_{i,j}^{3N-6} \gamma_{ij}^{A} Q_i Q_j & \sum_{i,j}^{3N-6} \eta_{ij}^{AB} Q_i Q_j \\ \sum_{i,j}^{3N-6} \eta_{ij}^{AB} Q_i Q_j & \sum_{i,j}^{3N-6} \gamma_{ij}^{B} Q_i Q_j \end{pmatrix}\end{aligned} \tag{4}$$

where the potential constants above, κ_i^A, κ_i^B, κ_i^{AB}, γ_{ij}^A, γ_{ij}^B, η_{ij}^{AB}, are defined as,

$$\kappa_i^{A} = \langle \Psi_A | \left(\frac{\partial \hat{H}_e}{\partial Q_i} \right)_0 | \Psi_A \rangle \tag{5}$$

$$\kappa_i^{B} = \langle \Psi_B | \left(\frac{\partial \hat{H}_e}{\partial Q_i} \right)_0 | \Psi_B \rangle \tag{6}$$

$$\kappa_i^{AB} = \langle \Psi_A | \left(\frac{\partial \hat{H}_e}{\partial Q_i} \right)_0 | \Psi_B \rangle \tag{7}$$

$$\gamma_{ij}^{A} = \langle \Psi_A | \left(\frac{\partial^2 \hat{H}_e}{\partial Q_i \partial Q_j} \right)_0 | \Psi_A \rangle \tag{8}$$

$$\gamma_{ij}^{B} = \langle \Psi_B | \left(\frac{\partial^2 \hat{H}_e}{\partial Q_i \partial Q_j} \right)_0 | \Psi_B \rangle \tag{9}$$

$$\eta_{ij}^{AB} = \langle \Psi_A | \left(\frac{\partial^2 \hat{H}_e}{\partial Q_i \partial Q_j} \right)_0 | \Psi_B \rangle \tag{10}$$

where Ψ_A and Ψ_B are the adiabatic electronic wavefunctions. The subscripts A and B can be thought of as the symmetry labels for the components of the degenerate electronic state in an Abelian subgroup, while the subscript 0 indicates that derivatives are evaluated at the conical intersection point.

(Note that in eqns. (5)–(10), we have given the leading terms, so that the definition of the gradient is clear. However, the full contribution to the gradient, including the second-order changes in energy due to first-order changes in the wavefunction, is actually computed). The first term in eqn. (4) is just a standard harmonic oscillator representation for each state (*i.e.*, completely analogous to single Born–Oppenheimer surface vibrational analysis[69,70]). Note that there are three types of constant, two diagonal and one off-diagonal, at first-order (involving the first derivative with respect to Q), and three types of constant at second-order (involving second derivatives with respect to Q). Depending on the particular Jahn–Teller symmetry, these three types of constant will be related to one another. The expansion in eqn. (4) is written as a zeroth-order term, which is chosen so that states are degenerate and have the same curvature (ω_i), plus a linear term, in which the degeneracy is lifted by terms proportional to the first derivatives, plus a quadratic term, in which the degeneracy is lifted by terms proportional to the second derivatives. In eqn. (4) ω_i is known as the unperturbed frequency of each mode.[26,28] These are arbitrary parameters as any changes can be compensated by changes in the second-order coefficients γ_{ij}^{A} and γ_{ii}^{B}. They are however useful in an interpretive context, and form a link to the standard quadratic Jahn–Teller Hamiltonian. This will become clear as the theory is developed below. The first-order terms (eqns. (5)–(7)) shift the harmonic parabolas from the origin, while the second-order terms (eqns. (8)–(10)) alter the curvature of each surface and give rise to the lifting of the degeneracy at second-order.

The symmetries of the modes that give non-zero potential constants above can be determined using group theoretical arguments (see ref. 26 and the appendix). The direct products of the irreps spanned by each component of the electronic state and those irreps spanned by the vibrational coordinates must contain the totally symmetric representation, or the matrix element is identically zero. These direct products are tabulated for all degenerate electronic states of all non-Abelian point groups.[26]

We now proceed to introduce an alternative set of vibrational coordinates that arises almost naturally from the usual treatment of conical intersections,[45,52,53,64]

$$\bar{\boldsymbol{Q}} = (\bar{Q}_{x_1},\bar{Q}_{x_2}) \oplus (\bar{Q}_1,\ldots,\bar{Q}_{3N-8}) \qquad (11)$$

This set of coordinates is spanned by the 'branching space': the mass-weighted gradient difference vector ($\bar{Q}_{x_1}$) and the mass-weighted interstate coupling vector ($\bar{Q}_{x_2}$), and the 'intersection space', whose coordinates are obtained as the normal modes of the projected Hessian ($\bar{Q}_1,\ldots,\bar{Q}_{3N-8}$). As discussed above, in this set of coordinates all of the terms which lift the degeneracy to first-order are contained within the 'branching space' spanned by ($\bar{Q}_{x_1}$) and ($\bar{Q}_{x_2}$).

At this point let us reiterate that the above coordinate system (eqn. (11)) is based upon the von Neumann–Wigner theorem. This type of vibrational coordinate system was originally introduced by Atchity, Xantheas and Ruedenberg,[60] termed 'intersection adapted coordinates', and has been extensively used by Yarkony.[45,52,53,71] Our methodology introduces an explicit representation for the $3N-8$ intersection space. Thus, from the von Neumann–Wigner theorem there are two and only two coordinates which lift the degeneracy at first-order in nuclear displacements. These coordinates are not constant for the seam of intersection but rather change continuously along the seam, as will be discussed later. The so-called multi-mode Jahn–Teller problem[47,50,65,72–74] arises because a given set of symmetry-adapted vibrational normal coordinates may not include any coordinates exactly parallel to the two vectors given above (eqns. (1) and (2)); this is not the case with the coordinate system in eqn. (11), and as we shall show the multi-mode problem is equivalent to determining the curvilinear seam from the rectilinear coordinates given in eqn. (11). Thus, the two equivalent (and complementary) views of the multi-mode Jahn–Teller problem can be summarised as: (i) using a fixed set of symmetry-adapted normal modes (taken from a related system in its equilibrium geometry) one can determine first- and second-order coupling constants for all modes of appropriate symmetry, or (ii) using 'intersection adapted co-ordinates' only two coordinates have a first-order coupling constant, however these coordinates change in a curvilinear manner along the seam, and may be combined with the local intersection space coordinates to determine a finite portion of the (curved) seam.

We shall rewrite eqn. (4) in terms of the 'intersection adapted' coordinate system,

$$\boldsymbol{V} = \begin{pmatrix} \frac{1}{2}\sum_{i}^{3N-6}\omega_i\bar{Q}_i^2 & 0 \\ 0 & \frac{1}{2}\sum_{i}^{3N-6}\omega_i\bar{Q}_i^2 \end{pmatrix} + \begin{pmatrix} \kappa_1^{A}\bar{Q}_{x_1} & \kappa_1^{AB}\bar{Q}_{x_2} \\ \kappa_1^{AB}\bar{Q}_{x_2} & \kappa_1^{B}\bar{Q}_{x_1} \end{pmatrix} + \begin{pmatrix} \sum_{i,j}^{3N-6}\gamma_{ij}^{A}\bar{Q}_i\bar{Q}_j & \sum_{i,j}^{3N-6}\eta_{ij}^{AB}\bar{Q}_i\bar{Q}_j \\ \sum_{i,j}^{3N-6}\eta_{ij}^{AB}\bar{Q}_i\bar{Q}_j & \sum_{i,j}^{3N-6}\gamma_{ij}^{B}\bar{Q}_i\bar{Q}_j \end{pmatrix} \qquad (12)$$

Notice that the summations have been removed from the linear term. Thus κ_1^{A} is the gradient on state A and κ_1^{AB} is the magnitude of the interstate coupling vector.

We now introduce a simple one-dimensional model example (adapted from ref. 75), where $\bar{Q}_{x_1}$ is the gradient difference coordinate, and $\kappa_1^{A} = \kappa$ in eqn. (12). This is known as the E $\otimes$ β Jahn–Teller problem (a degenerate E-type electronic state interacting with a single non-degenerate vibration), which occurs in some condensed phase systems. The E $\otimes$ β potential can be considered the limiting case of the E $\otimes$ ($b_1 \oplus b_2$) potential (*vide infra*) in which one of the linear coupling constants (eqns. (5)–(7)) is much larger than the other. The potential matrix is,

$$\boldsymbol{V} = \begin{pmatrix} \frac{1}{2}\omega\bar{Q}_{x_1}^2 & 0 \\ 0 & \frac{1}{2}\omega\bar{Q}_{x_1}^2 \end{pmatrix} + \begin{pmatrix} \kappa\bar{Q}_{x_1} & 0 \\ 0 & -\kappa\bar{Q}_{x_1} \end{pmatrix} \qquad (13)$$

Eqn. (13) is written as the sum of two matrices, zeroth-order (unperturbed harmonic oscillator) and first-order (linear

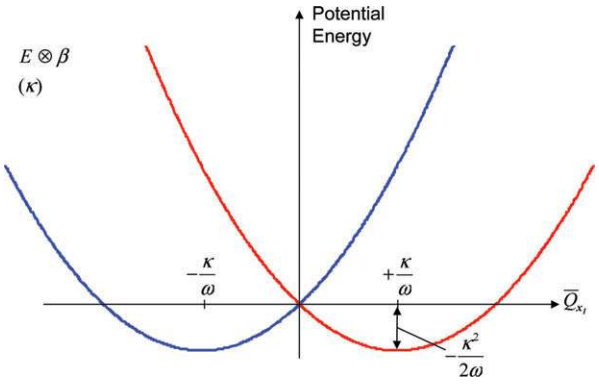

Fig. 2 One-dimensional potential energy curves obtained from the E $\otimes$ β Jahn–Teller Hamiltonian including linear coupling.

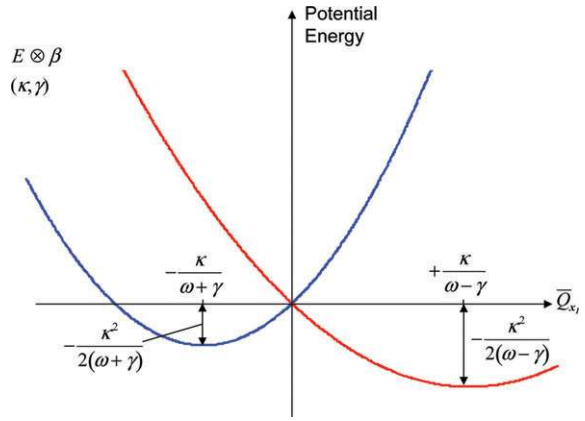

Fig. 3 One-dimensional potential energy curves obtained from the E ⊗ β Jahn–Teller Hamiltonian including linear and quadratic coupling.

coupling), and gives the following two expressions for the potential surfaces,

$$V^{+} = \frac{1}{2}\omega\bar{Q}_{x_1}^2 + \kappa\bar{Q}_{x_1} \tag{14}$$

$$V^{-} = \frac{1}{2}\omega\bar{Q}_{x_1}^2 - \kappa\bar{Q}_{x_1} \tag{15}$$

Plotting the solutions of eqns. (14) and (15) as a function of $\bar{Q}_{x_1}$ we obtain the potential energy curves shown in Fig. 2. The gradient at $\bar{Q}_{x_1} = 0$ is obviously $+\kappa$ or $-\kappa$, and the curvature of each surface is ω. The length of the gradient difference is 2κ. Thus, the term linear in Q in eqn. (13) has the effect of shifting two equivalent parabolas from $\bar{Q}_{x_1} = 0$ to $\bar{Q}_{x_1} = +\kappa/\omega$ and $\bar{Q}_{x_1} = -\kappa/\omega$ with a minimum energy of $-\kappa^2/2\omega$. The effect of quadratic coupling is shown in Fig. 3, where the curvature of each surface changes and two different minima occur.

Now we add the second dimension (coordinate $\bar{Q}_{x_2}$, the interstate coupling vector) to produce a circular cone (in the 'branching space' $\bar{Q}_{x_1}$ and $\bar{Q}_{x_2}$ with $\kappa = \kappa_1^{\mathrm{A}} = \kappa_1^{\mathrm{B}} = \kappa_2^{\mathrm{AB}}$),

$$\boldsymbol{V} = \begin{pmatrix} \frac{1}{2}\omega\bar{Q}_{x_1}^2 + \frac{1}{2}\omega\bar{Q}_{x_2}^2 & 0 \\ 0 & \frac{1}{2}\omega\bar{Q}_{x_1}^2 + \frac{1}{2}\omega\bar{Q}_{x_2}^2 \end{pmatrix} + \begin{pmatrix} \kappa\bar{Q}_{x_1} & \kappa\bar{Q}_{x_2} \\ \kappa\bar{Q}_{x_2} & -\kappa\bar{Q}_{x_1} \end{pmatrix} \tag{16}$$

Notice the term in $\bar{Q}_{x_2}$ that appears on the off-diagonal. The above potential matrix describes the E ⊗ e Jahn–Teller case,

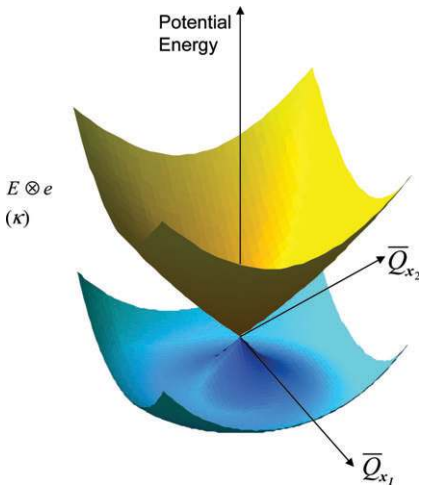

Fig. 4 Two-dimensional circular cone obtained from the E ⊗ e Jahn–Teller Hamiltonian including linear coupling.

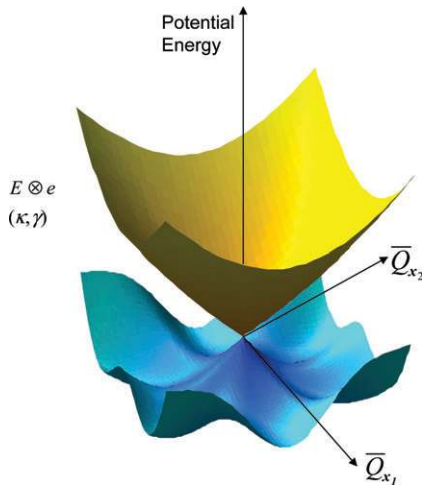

Fig. 5 Two-dimensional circular cone obtained from the E ⊗ e Jahn–Teller Hamiltonian including linear and quadratic coupling.

which is the prototypical circular cone shown in Fig. 4. The coordinates used are equivalent in this example because they transform as an E irrep of the point group, *i.e.*, the gradient difference and interstate coupling vectors can be interchanged due to the symmetry of the system. If quadratic coupling is included the effect is to produce 'bumps' in the Jahn–Teller 'moat' (see Fig. 5). The number of minima in the 'moat' depends on the largest C_n rotation axis of the point group. Notice that the saddle-points in the moat in Fig. 5 are the result of quadratic coupling within the 'branching space', *i.e.*, different curvatures of the potential surface along the gradient difference (eqn. (1)) and interstate coupling (eqn. (2)) coordinates.

If the 'branching space' is expressed in polar coordinates *i.e.*, a radial coordinate ρ and an angular coordinate ϑ, then the form of the potential surfaces obtained from eqn. (16) is expressed as,[28]

$$V^{\pm} = \frac{1}{2}K\rho^2 \pm [\kappa\rho + \gamma\rho^2\cos(n\vartheta)] \tag{17}$$

where n is an integer and corresponds to the largest C_n rotation axis, and,

$$K = (4\pi^2 Mc^2)\omega^2 \tag{18}$$

where M is the reduced mass of the mode, c is the speed of light and ω is the zeroth-order unperturbed vibrational frequency discussed above. Obviously if the second-order coupling (γ) is zero, then the surfaces are those of a double-cone (the lower state surface being the famous 'mexican hat' potential). The inclusion of a non-zero γ causes 'bumps' in the 'trough' of the moat. In Fig. 5 this is shown for a six-fold rotation axis, for example the benzene radical cation. The standard form of polar coordinates used in Jahn–Teller studies is the complex combination. For the 'branching space' this is,

$$\rho e^{\pm i\vartheta} = \bar{Q}_{x_1} \pm i\bar{Q}_{x_2} \tag{19}$$

This form is particularly useful for decomposing degenerate irreducible representations (irreps) in the C_n subgroup (*i.e.*, the subgroup of pure rotations), since degenerate irreps appear in complex conjugate pairs in these groups.[76]

Returning now to the linear potential (eqn. (16)), but reducing the symmetry: the potential matrix given in eqn. (20) is the eqn. for an elliptic cone (when the gradient difference and interstate coupling vectors cannot be interchanged). If we restrict the expansion to the 'branching space' and when

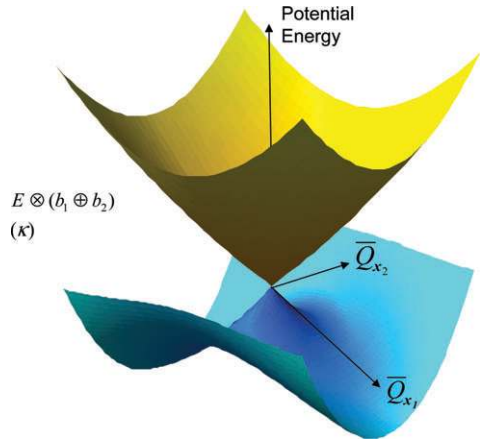

Fig. 6 Two-dimensional elliptic cone obtained from the E ⊗ (b_1 ⊕ b_2) linear vibronic coupling Jahn–Teller Hamiltonian.

$\kappa_1^{\mathrm{A}} = \kappa_1^{\mathrm{B}} = \kappa_1$,

$$\boldsymbol{V} = \begin{pmatrix} \frac{1}{2}\omega\bar{Q}_{x_1}^2 + \frac{1}{2}\omega\bar{Q}_{x_2}^2 & 0 \\ 0 & \frac{1}{2}\omega\bar{Q}_{x_1}^2 + \frac{1}{2}\omega\bar{Q}_{x_2}^2 \end{pmatrix} + \begin{pmatrix} \kappa_1\bar{Q}_{x_1} & \kappa_2^{\mathrm{AB}}\bar{Q}_{x_2} \\ \kappa_2^{\mathrm{AB}}\bar{Q}_{x_2} & -\kappa_1\bar{Q}_{x_1} \end{pmatrix} \tag{20}$$

This example corresponds to an E ⊗ (b_1 ⊕ b_2) Jahn–Teller system, *i.e.*, a degenerate electronic state (transforming as the E representation of the point group) has its degeneracy lifted to first-order by vibrations of b_1 and b_2 symmetry. This occurs in molecules where the principal axis of symmetry is C_4, and in such cases the gradient difference transforms as b_1 and the interstate coupling as b_2 (or *vice versa* dependent upon a unitary transformation of the states). Note that along $\bar{Q}_{x_2}$, the local minimum is actually a saddle point in the space of both coordinates: the distortion along one coordinate does not produce the same shift as along the other, because the value of κ is not the same for both coordinates (see Fig. 6). For the E ⊗ (b_1 ⊕ b_2) Jahn–Teller system, saddle points occur in the 'moat' even at the linear vibronic coupling level *i.e.*, when terms proportional to first derivatives lift the degeneracy. If quadratic coupling is included, additional minima may occur.

The quadratic terms in the potential matrix lift the degeneracy at second-order. Let us consider an E ⊗ e Jahn–Teller system. Let us choose two of the $3N - 8$ coordinates that define the 'intersection space' as $\bar{Q}_a$ and $\bar{Q}_b$. For the E ⊗ e Hamiltonian the pair $\bar{Q}_a$, $\bar{Q}_b$ must be components of a degenerate vibrational mode. For these modes, which are not Jahn–Teller active modes as they are in the intersection space, we have,

$$\boldsymbol{V} = \begin{pmatrix} \frac{1}{2}\omega\bar{Q}_a^2 + \frac{1}{2}\omega\bar{Q}_b^2 & 0 \\ 0 & \frac{1}{2}\omega\bar{Q}_a^2 + \frac{1}{2}\omega\bar{Q}_b^2 \end{pmatrix} + \begin{pmatrix} \gamma^{\mathrm{A}}(\bar{Q}_a^2 + \bar{Q}_b^2) & \eta^{\mathrm{AB}}\bar{Q}_a\bar{Q}_b \\ \eta^{\mathrm{AB}}\bar{Q}_a\bar{Q}_b & \gamma^{\mathrm{B}}(\bar{Q}_a^2 + \bar{Q}_b^2) \end{pmatrix} \tag{21}$$

where ω is the frequency of each component of the degenerate vibration before the splitting (equal at zeroth-order). The γ terms split the frequency of the mode to give frequencies of $\omega + \gamma^{\mathrm{A}}$ and $\omega + \gamma^{\mathrm{B}}$. Thus the difference in the γ terms lifts the degeneracy at second-order. In the absence of the second term in eqn. (21) each surface would have the same curvature and they would remain degenerate along either $\bar{Q}_a$ or $\bar{Q}_b$. For practical reasons we now neglect the off-diagonal[77,78] terms involving $\bar{Q}_a\bar{Q}_b$. The rationale behind this approximation is discussed in ref. 41. In this context, we note that the bilinear couplings η_{ij}^{AB} along the branching-space modes are also neglected, although it has been argued that these terms have to be included in the second-order expansion to reproduce Jahn–Teller spectra accurately.[108,109] These terms can be obtained from the calculated CASSCF Hessians, and future extensions of our work will include their evaluation. However, we note that our topological analysis, which is based on calculating the curvature of the seam, is not significantly affected by these terms, since our characterization of the higher-symmetry conical intersection points of fulvene and the cyclopropenyl radical as 'saddle points in the degenerate space' is confirmed by the optimization of lower-energy points of degeneracy with lower symmetry.

In summary, our vibrational coordinate basis (eqn. (11)) has the following properties: (1) the linear coupling is contained solely within the 'branching space' and is not spread over several modes with the same symmetry, and (2) the differences in the harmonic frequencies for degenerate vibrational modes gives the quadratic coupling constants for a representation of the 'intersection space' based on the projected state-averaged Hessian for each component of the degenerate electronic state.

Using first- and second-order potential constants to represent the seam

In this section we briefly review the concept of the conical intersection seam, and in particular, how a representation can be obtained using the first- and second-order potential constants (eqns. (5)–(10) above). The following is a brief summary of the key equations developed in ref. 41. We then use this methodology to determine a portion of the E ⊗ e seam in the cyclopropenyl radical, and show that the D_{3h} Jahn–Teller point is in fact a third-order saddle-point on the seam of intersection. We refer to ref. 41 for a detailed mathematical discussion of the seam curvature.

Eqn. (12) above can be written as,

$$\boldsymbol{V} = \boldsymbol{E} + \begin{pmatrix} \kappa^{\mathrm{A}}\bar{Q}_{x_1} & \kappa^{\mathrm{AB}}\bar{Q}_{x_2} \\ \kappa^{\mathrm{AB}}\bar{Q}_{x_2} & \kappa^{\mathrm{B}}\bar{Q}_{x_1} \end{pmatrix} + \begin{pmatrix} \sum_{a\in\mathrm{BS}} \gamma_a^{\mathrm{A}}\bar{Q}_a^2 & 0 \\ 0 & \sum_{a\in\mathrm{BS}} \gamma_a^{\mathrm{B}}\bar{Q}_a^2 \end{pmatrix} + \begin{pmatrix} \sum_{b\in\mathrm{IS}} \gamma_b^{\mathrm{A}}\bar{Q}_b^2 & 0 \\ 0 & \sum_{b\in\mathrm{IS}} \gamma_b^{\mathrm{B}}\bar{Q}_b^2 \end{pmatrix} \tag{22}$$

where $\boldsymbol{E}$ is a diagonal matrix with diagonal elements equal to E_{A}^0 and E_{B}^0 (energies at the conical intersection point). In eqn. (22) above, we have neglected any cross-quadratic coupling terms and any second-order interstate coupling. Diagonalisation of $\boldsymbol{V}$ yields a quadratic representation of the potential surfaces in the vicinity of the conical intersection.

$$E_{\mathrm{A,B}} = \lambda\bar{Q}_{x_1} + \sum_{a\in\mathrm{BS}} \omega_a\bar{Q}_a^2 + \sum_{b\in\mathrm{IS}} \omega_b\bar{Q}_b^2 \pm \frac{1}{2}\sqrt{\left(\delta\kappa\bar{Q}_{x_1} + \sum_{a\in\mathrm{BS}} \delta\gamma_a\bar{Q}_a^2 + \sum_{b\in\mathrm{IS}} \delta\gamma_b\bar{Q}_b^2\right)^2 + \left(2\kappa^{\mathrm{AB}}\bar{Q}_{x_2}\right)^2} \tag{23}$$

$$\lambda = (\kappa^{\mathrm{B}} + \kappa^{\mathrm{A}})/2 \tag{24}$$

$$\delta\kappa = \kappa^{\mathrm{B}} - \kappa^{\mathrm{A}} \tag{25}$$

$$\omega_i = (\gamma_i^{\mathrm{B}} + \gamma_i^{\mathrm{A}})/2 \tag{26}$$

$$\delta\gamma_i = \gamma_i^{\mathrm{B}} - \gamma_i^{\mathrm{A}} \tag{27}$$

where we have dropped the redundant double lower index on the γ terms.

Thus the energy difference between the two states is

$$\Delta E = \sqrt{\left(\delta\kappa\bar{Q}_{x_1} + \sum_{a\in\mathrm{BS}}\delta\gamma_a\bar{Q}_a^2 + \sum_{b\in\mathrm{IS}}\delta\gamma_b\bar{Q}_b^2\right)^2 + \left(2\kappa^{\mathrm{AB}}\bar{Q}_{x_2}\right)^2} \tag{28}$$

The conical intersection seam is defined as the locus of points where the two electronic states remain degenerate, *e.g.*, both components of an E state in a Jahn–Teller molecule. Setting the energy difference (eqn. (28)) to zero (and neglecting the second-terms in the 'branching space'), we obtain eqn. (29) that defines the seam in terms of 'branching space' (BS) and 'intersection space' (IS) coordinates, *i.e.*, the rectilinear set computed by our frequency analysis.

$$\left(\delta\kappa\bar{Q}_{x_1} + \sum_{b\in\mathrm{IS}}\delta\gamma_b\bar{Q}_b^2\right)^2 + \left(2\kappa^{\mathrm{AB}}\bar{Q}_{x_2}\right)^2 = 0 \tag{29}$$

In order to concentrate on the curvilinear nature of the seam we now assume that the two terms in parentheses on the left of eqn. (29) are linearly independent. This is rigorously true for all of the examples studied in this paper; indeed it is always true if the two degenerate electronic states transform as different irreducible representations of some non-Abelian point-group (see ref. 41 for a discussion of this). Thus the seam is a combination of the gradient difference coordinate and the rectilinear 'intersection space' coordinates, *i.e.*,

$$\delta\kappa\bar{Q}_{x_1} + \sum_{b\in\mathrm{IS}}\delta\gamma_b\bar{Q}_b^2 = 0 \tag{30}$$

As we have shown elsewhere,[41] the seam has the local geometry of a hypercurve. Eqn. (30) is the eqn. of a paraboloid, while the seam is locally a central (hyper)conic section (a hyperboloid or an ellipsoid) when the second-order splitting in the 'branching space' is also included. There are $3N-8$ linearly independent solutions to eqn. (30), *i.e.*,

$$\delta\kappa\bar{Q}_{x_1} + \delta\gamma_i\bar{Q}_i^2 = 0 \qquad i\in\mathrm{IS} \tag{31}$$

Each curvilinear coordinate is now obtained as a solution to eqn. (31). The curvilinear coordinate transformation from the rectilinear to the seam coordinates (t_i) is obtained by writing eqn. (31) in terms of a parameter t for each of the $3N-8$ pairs of solutions,

$$\bar{Q}_{x_1} = -\frac{1}{\delta\kappa}t_i^2 = -\alpha t_i^2 \qquad \alpha = \frac{1}{\delta\kappa} \tag{32}$$

$$\bar{Q}_i = \frac{1}{\sqrt{\delta\gamma_i}}t_i = \beta_i t_i \qquad \beta_i = \frac{1}{\sqrt{\delta\gamma_i}} \tag{33}$$

The expression for the energy of one of the states along the $\bar{Q}_{x_1}$ and $\bar{Q}_i$ coordinates is obtained from eqn. (28) and is,

$$\begin{aligned} E_{\mathrm{seam}} &= \lambda\bar{Q}_{x_1} + \gamma_1\bar{Q}_{x_1}^2 + \gamma_i\bar{Q}_i^2 + \delta\kappa\bar{Q}_{x_1} + \delta\gamma_i\bar{Q}_i^2 \\ &= \kappa^{\mathrm{A}}\bar{Q}_{x_1} + \gamma_1^{\mathrm{A}}\bar{Q}_{x_1}^2 + \gamma_i^{\mathrm{A}}\bar{Q}_i^2 \quad i\in\mathrm{IS} \end{aligned} \tag{34}$$

Substituting from eqns. (32) and (33) we have,

$$\begin{aligned} E_{\mathrm{seam}} &= -\alpha\kappa^{\mathrm{A}}t_i^2 + \gamma_1^{\mathrm{A}}\alpha^2t_i^4 + \gamma_i^{\mathrm{A}}\beta^2t_i^2 = \gamma_1^{\mathrm{A}}\alpha^2t_i^4 \\ &\quad + (\gamma_i^{\mathrm{A}}\beta_i^2 - \alpha\kappa^{\mathrm{A}})t_i^2 \qquad i\in\mathrm{IS} \end{aligned} \tag{35}$$

Eqn. (35) gives the energy of the states along a degeneracy-retaining coordinate t_i. We refer to it as the energy of the intersection seam (hyperline) along the curved coordinate t_i.

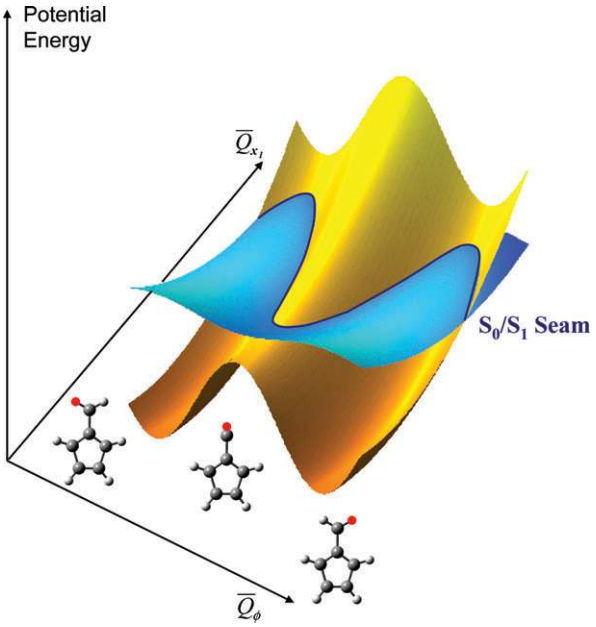

Fig. 7 The S_0–S_1 seam of intersection in fulvene (adapted from ref. 41).

The expression required to characterize the curvature of the hyperline is then,

$$\left(\frac{\partial^2 E}{\partial t_i^2}\right)_{t=0} = 2(\gamma_i^{\mathrm{A}}\beta_i^2 - \kappa^{\mathrm{A}}\alpha) = 2\left\{\left(\frac{\gamma_i^{\mathrm{A}}}{\delta\gamma_i}\right) - \left(\frac{\kappa^{\mathrm{A}}}{\delta\kappa}\right)\right\} \tag{36}$$

Thus a knowledge of the first- and second-order terms in eqn. (36) are sufficient to determine if an optimized point on the degenerate hyperline is a minimum or saddle point.

In ref. 41 we have used the above analysis to map the S_0–S_1 seam of intersection in fulvene. In fulvene, we find that the planar intersection is a second-order saddle point on the seam, and that there are two separate branches of the seam leading to lower symmetry critical points of C_2 and C_s symmetry. These points represent minima on the seam, with the C_2 point being the global minimum on the seam. Part of the seam of intersection is shown in Fig. 7. The S_0 and S_1 adiabatic potential surfaces are plotted against the gradient difference coordinate ($\bar{Q}_{x_1}$) and the methylenic torsion coordinate ($\bar{Q}_\phi$). The curved nature of the seam is apparent from Fig. 7; this curvature arises from the fact that a combination of first- and second-order coordinates is needed to preserve the degeneracy.

Obviously this type of analysis holds at Jahn–Teller points as well, and the surprising result is that a high-symmetry Jahn–Teller crossing can be a saddle-point on the seam. The cyclopropenyl radical is an example of this, where two separate degeneracy-preserving coordinates lead to lower-energy C_{3v} and C_s minima on the seam.

Computational details

To determine the second-order effects, we project the 'branching space' from the full $3N$-dimensional Hessian for each state. The projection technique is based on that first used by Baboul and Schlegel[79] to compute vibrational frequencies orthogonal to a reaction path. The projected Hessian $\bar{\boldsymbol{H}}$ is given by,

$$\bar{\boldsymbol{H}} = \boldsymbol{P}^\dagger\boldsymbol{H}^{\mathrm{MW}}\boldsymbol{P} \tag{37}$$

where $\boldsymbol{H}^{\mathrm{MW}}$ is the mass-weighted Cartesian Hessian and $\boldsymbol{P}$ is the following projection matrix,

$$\begin{aligned} \boldsymbol{P} = 1 &- \boldsymbol{t}_x\boldsymbol{t}_x^{\mathrm{T}} - \boldsymbol{t}_y\boldsymbol{t}_y^{\mathrm{T}} - \boldsymbol{t}_z\boldsymbol{t}_z^{\mathrm{T}} - \boldsymbol{r}_a\boldsymbol{r}_a^{\mathrm{T}} - \boldsymbol{r}_b\boldsymbol{r}_b^{\mathrm{T}} - \boldsymbol{r}_c\boldsymbol{r}_c^{\mathrm{T}} \\ &- \boldsymbol{x}_1\boldsymbol{x}_1^{\mathrm{T}} - \boldsymbol{x}_2\boldsymbol{x}_2^{\mathrm{T}} \end{aligned} \tag{38}$$

where the vectors corresponding to translation of the centre of mass ($\boldsymbol{t}_i$), and rotation around the principal axes of inertia

(***a***, ***b*** and ***c***) are given by,

$$\boldsymbol{t}_x = \frac{1}{\sqrt{m_i}}(1,0,0,1,0,0,...,1,0,0)^{\mathrm{T}} \quad (39)$$

$$\boldsymbol{t}_y = \frac{1}{\sqrt{m_i}}(0,1,0,0,1,0,...,0,1,0)^{\mathrm{T}} \quad (40)$$

$$\boldsymbol{t}_z = \frac{1}{\sqrt{m_i}}(0,0,1,0,0,1,...,0,0,1)^{\mathrm{T}} \quad (41)$$

$$(\boldsymbol{r}_a)_{ij} = \frac{((W_y)_i X_{j,3} - (W_z)_i X_{j,2}}{\sqrt{m_i}} \quad (42)$$

$$(\boldsymbol{r}_b)_{ij} = \frac{((W_z)_i X_{j,1} - (W_x)_i X_{j,3}}{\sqrt{m_i}} \quad (43)$$

$$(\boldsymbol{r}_c)_{ij} = \frac{((W_x)_i X_{j,2} - (W_y)_i X_{j,1}}{\sqrt{m_i}} \quad (44)$$

where $j = x, y, z$ and i runs over all nuclei; W is the dot product of the centre of mass vector with the corresponding row of the inertia tensor (for details see the classic treatise on vibrational spectroscopy by Wilson *et al*.,[69] and for details of the standard vibrational analysis in *Gaussian*[80] see ref. 81). The 'branching space' is thus projected from the Hessian in the same manner as the translational and rotational modes are normally projected during a single surface Born–Oppenheimer harmonic vibrational frequency analysis. The state-averaged Hessian matrix is expensive to compute, but this is available from a conical intersection optimization provided the coupled-perturbed MCSCF (CP-MCSCF) eqns. are solved. For details on the computation of state-averaged second-derivatives see ref. 82.

All computations were performed using SA-CASSCF with the aug-cc-pVTZ basis for the HCCS radical and the cc-pVDZ basis set for the C_nH_n radicals. For HCCS, the active space consisted of the six π-orbitals plus the σ-lone pair orbital of the sulfur. There are seven π-electrons plus the two electrons of the lone-pair giving an (9,7) active space. For the C_nH_n radicals the unambiguous choice of active spaces consisted of the p_π-electrons distributed in the p_π-orbitals. Thus for C_3H_3 a (3,3) active space was used, for $C_4H_4^+$ a (3,4) active space was used, while for C_5H_5 (Cp) a (5,5) active space was used. All computations were performed on an IBM SP2 using a development version of the *Gaussian*[80] program.

The Renner–Teller effect in HCCS

An example of a frequency analysis of a linear molecule exhibiting the Renner–Teller effect[61,63] provides a useful introduction to the frequency analysis of the 'intersection space' at a conical intersection. In a Renner–Teller active molecule the degeneracy of electronic states is not lifted to first-order in nuclear displacements and there is no conical intersection.[47,61,62] Rather, there is a 'glancing' or 'touching' of the two surfaces. Indeed Herzberg[62] suggested that Renner–Teller geometries should be referred to as 'glancing intersections'. It can be shown using simple group theoretical arguments that there is no linear vibronic coupling term in the expansion in eqn. (4) given above for linear molecules belonging to the $C_{\infty v}$ and $D_{\infty h}$ point-groups (see for example ref. 83). Thus, the optimized linear geometries are simultaneously critical points on both surfaces and can be optimized and characterized using standard analytical derivative techniques. The $3N - 5$ frequencies and normal modes for each surface of a Renner–Teller system are analogous to the frequencies and normal modes in the projected $(3N - 8)$-dimensional space at an optimized conical intersection. We are able to rationalize the Renner–Teller topology with simple valence bond electronic structure arguments. The degenerate $\tilde{X}\ ^2\Pi$ and $A\ ^2\Pi$ states of the HCCS molecule illustrate some general concepts with regards to the second-order degeneracy lifting.

The $3N - 5$ normal modes for each surface at a Renner–Teller point are equivalent. Likewise, the set of frequencies for one surface also match those of the other surface. The Renner–Teller effect manifests itself in the fact that the frequency of a component of a degenerate bending vibration on one surface is the same as the frequency of the other component of the bending vibration on the other surface. Let us consider this in more detail. The molecule is linear, and we shall orientate it such that the *z*-axis coincides with the inter-nuclear axis. Bending vibrations can therefore take place in the *xz*- or *yz*-planes, and each of these motions is completely equivalent. The bending vibrations therefore transform as degenerate Π representations of the point group ($C_{\infty v}$ or $D_{\infty h}$). The normal mode and frequency of the *xz*-component of a bending vibration for one of the electronic states exactly matches that for the *yz*-component of the bending vibration for the other electronic state. However, the *xz*-bending mode and frequency are different from the *yz*-bending for the same electronic state.[84] This is a very general property of Renner–Teller surfaces, which we later show also occurs for the 'intersection space' at an optimized Jahn–Teller conical intersection. Thus if we plot the energy as a function of one of the components of a bending vibration the degeneracy is lifted, since the frequency for the bending is different on each surface (Fig. 1).

If the frequencies on both surfaces are real, they both have positive curvature and the potential energy curves along a bending mode have the form of two parabolas with coincidental minima but having different curvatures (see Fig. 1, Renner–Teller type-I). If the frequencies on both surfaces are imaginary, they both have negative curvature and the potential energy curves have two coincidental maxima (see Fig. 1, Renner–Teller type-III). The final type of topology occurs when one surface has a minimum at the linear geometry, while the other has a saddle point (see Fig. 1, Renner–Teller type-II). In this case one frequency is real while the other is imaginary. For a detailed discussion on the five unique Renner–Teller surface topologies we refer the reader to refs. 63 and 85.

The ground electronic state ($\tilde{X}\ ^2\Pi$) and first excited state ($A\ ^2\Pi$) of HCCS are each orbitally degenerate doublets,[86,87] and exhibit a Renner–Teller effect. However, the topology of the Renner–Teller surface is different in each case. The ground state shows a type-I topology for both degenerate bending vibrations, while the excited state shows a type-III topology along one bending vibration and type-I topology along the other. The different topologies can be rationalized by considering the electronic structure of each state. The electronic

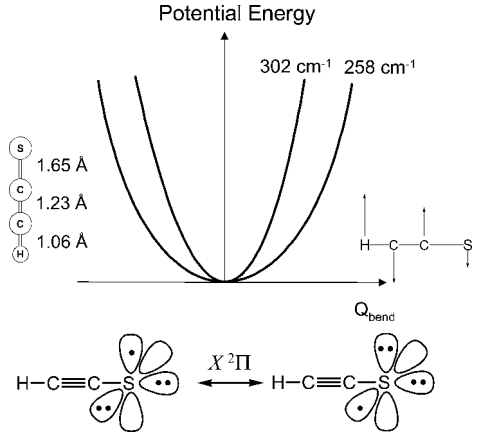

Fig. 8 Renner–Teller potential energy surface topology for the degenerate $\tilde{X}\ ^2\Pi$ ground state of HCCS. The topology is Renner–Teller type-I *i.e*., both surfaces have a positive force constant with respect to the bending vibration shown.

Table 1 HCCS: CAS(9,7)/aug-cc-pvTZ energetics

Geometry	State	Energy/E_h	Rel. energy/ kJ mol^{-1}
Linear ground state	$\tilde{X}\ ^2\Pi$ (D_0/D_1)	−473.866 116	0.00
Linear vertically excited	A $^2\Pi$ (D_2/D_3)	−473.738 937	333.93
Linear relaxed SO saddle-point	A $^2\Pi$ (D_2/D_3)	−473.744 442	319.45
Bent minimum	D_2	−473.750 225	304.26
Bent minimum	D_3	−473.746 764	313.34

structure of the doubly degenerate $\tilde{X}\ ^2\Pi$ state is shown in Fig. 8. There is a triple bond between the carbon atoms, with the singly occupied orbital being either the sulfur p_x or p_y, giving rise to the degeneracy. The linear geometry of the $\tilde{X}\ ^2\Pi$ state was optimized using state-averaged orbitals and is given to the left hand side of Fig. 8. For the energetics see Table 1.

A state-averaged frequency analysis has been performed for both the D_0 and D_1 component states of $\tilde{X}\ ^2\Pi$. The $3N-5=7$ normal modes obtained for each state are identical. There are two degenerate bending vibrations (Π symmetry) and three non-degenerate stretching vibrations (Σ^+ symmetry). The frequencies for these modes on each surface are given in Table 2.[88] It should be noted that the set of frequencies exactly match one another on each surface, but within a degenerate bending mode the frequencies do not match. The Renner–Teller effect becomes apparent when the same bending vibration on both surfaces is compared. The first degenerate vibration (shown in Fig. 8) has two component frequencies of 258 cm^{-1} and 302 cm^{-1}. On D_0 these correspond to bending in the *yz*- and *xz*-planes respectively, while on D_1 they correspond to bending in the *xz*- and *yz*-planes. The modes therefore swap between the two surfaces.

Fig. 8 shows the potential energy curves for the D_0 and D_1 ($\tilde{X}\ ^2\Pi$) states along one component of the bending vibration. The surface topology is seen to be Renner–Teller type-I. This is consistent with the valence bond structure shown. The carbons are triply bonded in both electronic resonance structures, and upon any bending the energy will rise. The reason that the frequencies differ for each component of the bending vibration is that the degenerate electronic states have a lone pair and a singly occupied orbital. Bending towards the lone pair will raise the energy more sharply than bending towards the singly occupied orbital, due to the different electrostatic repulsions with the CC triple bond. The frequency for bending in the plane of the lone pair is therefore greater than that for bending in the plane of the singly occupied orbital. The second degenerate bending vibration shows the same effect with the same surface topology (and for the same reason). The stretching modes have the same frequencies on both surfaces. Therefore motion along these modes preserves the degeneracy to second-order in nuclear displacements. This is to be expected since the stretch modes maintain the orbitally degenerate linear geometry.

Table 2 State-averaged harmonic vibrational frequencies for the $\tilde{X}\ ^2\Pi$ state of HCCS at its optimized linear geometry

D_0			D_1		
ω/cm^{-1}	Symmetry ($C_{\infty v}$)	Vibration	ω/cm^{-1}	Symmetry ($C_{\infty v}$)	Vibration
Non-degenerate modes					
761	Σ^+	Stretch	761	Σ^+	Stretch
1993	Σ^+	Stretch	1993	Σ^+	Stretch
3619	Σ^+	Stretch	3619	Σ^+	Stretch
Degenerate modes					
258	Π	*yz*-bend	258	Π	*xz*-bend
302		*xz*-bend	302		*yz*-bend
373	Π	*yz*-bend	373	Π	*xz*-bend
557		*xz*-bend	557		*yz*-bend

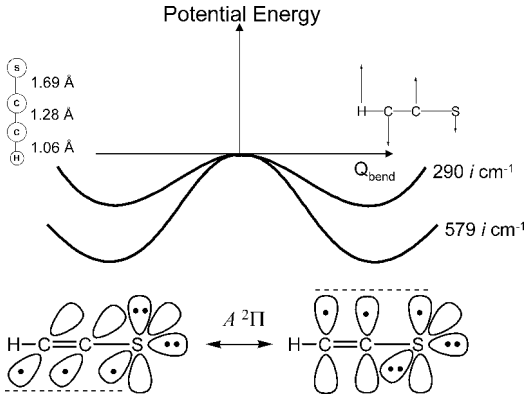

Fig. 9 Renner–Teller potential energy surface topology for the degenerate $A^2\Pi$ first excited state of HCCS. The topology is Renner–Teller type-III *i.e.*, both surfaces have a negative force constant with respect to the bending vibration shown.

The first excited state involves an excitation of the π-system ($9\sigma^2 2\pi^4 3\pi^3 \rightarrow 9\sigma^2 2\pi^3 3\pi^4$). This state can be represented by the valence bond structure shown in Fig. 9, while the optimized geometry is shown to the top left in the same figure. The carbon atoms are double bonded and there is a three-electron allyl like resonance between either the p_x or p_y orbitals of the two carbon atoms and the sulfur atom. This three-electron resonance provides the driving force for the type-III Renner–Teller topology of the first bending vibration, since stable minima exist on both the D_2 and D_3 surfaces with similar bent geometries (see Fig. 10). Indeed recent experimental and theoretical studies indicate that HCCS is bent in the first optically active excited state.[89]

The harmonic vibrational frequencies for both states are given in Table 3, which shows that the frequencies of both components of the first bending vibration are imaginary. The linear geometry is therefore simultaneously a second-order saddle-point on both D_2 and D_3 ($A^2\Pi$) surfaces. The mode swapping is again observed, 579i cm^{-1} for bending in the *xz* plane and 290i cm^{-1} for bending in the *yz*-plane on one surface, and the reverse on the other surface. The topology is therefore Renner–Teller type-III, and is shown in Fig. 9.

The E ⊗ e Jahn–Teller effect in the cyclopropenyl radical: a saddle-point and minimum Jahn–Teller points on the seam

To introduce some of the ideas discussed above in relation to the Jahn–Teller effect we proceed to discuss the cyclopropenyl radical. This molecule is a prototype system for the E ⊗ e Jahn–Teller effect in a molecule with several vibrational degrees of freedom. Indeed at D_{3h} geometries the symmetrical hydrogen

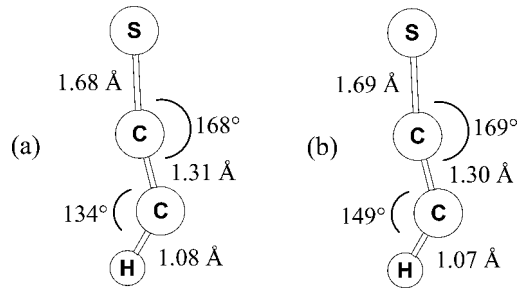

Fig. 10 State-averaged optimised geometries for the (a) D_2 and (b) D_3 states of HCCS. The existence of these minima provides the driving force for the Renner–Teller type-III topology of the $A\ ^2\Pi$ state at linear geometries.

Table 3 State-averaged harmonic vibrational frequencies for the A $^2\Pi$ state of HCCS at its optimized linear geometry[a]

D_2			D_3		
ω/cm^{-1}	Symmetry ($C_{\infty v}$)	Vibration	ω/cm^{-1}	Symmetry ($C_{\infty v}$)	Vibration
Non-degenerate modes					
795	Σ^+	Stretch	795	Σ^+	Stretch
2220	Σ^+	Stretch	2220	Σ^+	Stretch
3623	Σ^+	Stretch	3623	Σ^+	Stretch
Degenerate modes					
579i	Π	*yz*-Bend	579i	Π	*xz*-Bend
290i		*xz*-Bend	290i		*yz*-Bend
265	Π	*yz*-Bend	265	Π	*xz*-Bend
310		*xz*-Bend	310		*yz*-Bend

[a] $i = \sqrt{-1}$.

skeleton surrounding the C_3 shell can be seen as an extension from the thoroughly investigated triatomic (X_3) Jahn–Teller system.[47–49]

Before discussing the spectroscopic constants computed with our method we shall first of all determine the local minimum energy point on the Jahn–Teller seam. Surprisingly, the highly-symmetrical D_{3h} geometry is not the minimum on the seam, but rather a third-order saddle-point (see Fig. 11). At D_{3h} geometries the molecule exists in a $^2E''$ electronic state and is therefore Jahn–Teller unstable. It was previously assumed that the lowest energy D_{3h} geometry was a minimum on the seam of intersection. As we shall show this is not the case (compare the following results for the cyclopropenyl radical with those of the cyclobutadienyl radical cation and the cyclopentadienyl radical to follow).

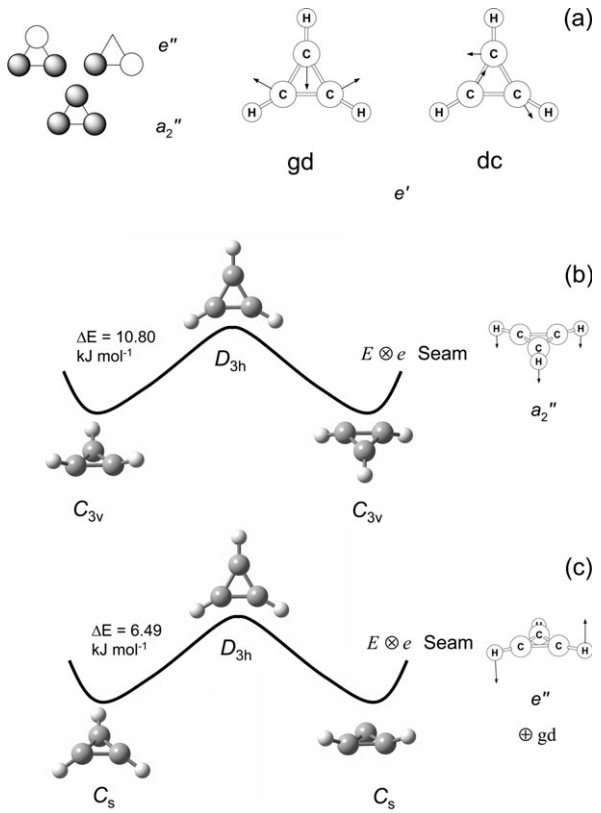

Fig. 11 (a) Cyclopropenyl radical: the degenerate Jahn–Teller state, shown with the gradient difference (gd) and interstate coupling (dc) vectors, which lift the degeneracy at first-order. (b) The curvilinear seam obtained as the non-degenerate out-of-plane vibration (a_2''), bilinearly coupled to the out-of-plane degenerate (e″) vibration, leading to the global minimum in the 'intersection space'. (c) The curvilinear seam obtained by combining the gd vector and the degenerate out-of-plane vibration (e″), leading to symmetry equivalent local minima in the 'intersection space'.

Using the group theoretical arguments discussed in the appendix the non-vanishing potential constants can be determined. In this example the first-order constants are non-zero only for vibrations symmetrical about the σ_h reflection plane. Thus the gradient difference and interstate coupling vectors lie in the molecular plane (and will span E′). The second-order potential constants however have no such restriction (since the direct product of two double-primed representations is a primed one). Our vibrational frequency analysis shows that the degenerate out-of-plane CH bending vibration has a Renner–Teller type-II topology for both vibrational components. This, together with eqn. (36) allows the curvature of the curvilinear seam to be determined. It follows that the D_{3h} geometry is in fact a third-order saddle-point on the seam.

The canonical vibrational normal coordinates at D_{3h} span the following irreps: $2A'_1 \oplus A'_2 \oplus 3E' \oplus A''_2 \oplus E''$. Note that there are three vibrations of E′ symmetry and if eqn. (4) was used (*i.e.* without separating first- and second-order contributions), then each of these can have non-zero linear potential constants. However if our alternative vibrational coordinate basis (eqn. (11)) is used then only one mode (*i.e.*, the $\bar{Q}_{x_1}$, $\bar{Q}_{x_2}$ pair) has a non-zero linear coupling constant. The quadratic-coupling constants are then obtained for all the remaining E modes (both E′ and E″). The values of the harmonic frequencies are given in Table 4. Note that there is a degenerate mode with a Renner–Teller type-II topology (Fig. 1). Thus this mode has a very large quadratic-coupling constant.

The global minimum energy point on the seam has C_{3v} symmetry and is shown in Fig. 11. This point is reached by following the a_2'' normal mode from the D_{3h} geometry, as shown in Fig. 11b. The values of the harmonic frequencies for this mode require some further comment. Obviously following the a_2'' bending mode from the D_{3h} Jahn–Teller point leads directly to a C_{3v} geometry (which is also a Jahn–Teller point, as C_{3v} is a non-Abelian point group). One would therefore expect the harmonic vibrational frequencies on each surface to be the same (*i.e.*, both imaginary but the same magnitude). Table 5 shows that this mode has a Renner–Teller type-III topology. This splitting is in fact caused by a bilinear coupling between the a_2'' mode and one component of the e″ mode. These two modes can couple since $A''_2 \otimes E'' = E'$, and since the symmetrized direct product of the electronic state irrep with itself is $[E'' \otimes E''] = E'$. In the C_{2v} subgroup $A_2'' \rightarrow B_1$ and $E'' \rightarrow A_2 \oplus B_1$, therefore it is the b_1 component of the e″ bending vibration which is coupled to the a_2'' vibration. The effect of this bilinear coupling is observed in the mixing of the two normal coordinates. In this case the a_2'' normal coordinate

Table 4 Projected state-averaged harmonic vibrational frequencies for the cyclopropenyl radical at D_{3h} and C_{3v} critical points on the E ⊗ e Jahn–Teller seam[a]

D_{3h}	D_0 ω/cm^{-1}	D_1 ω/cm^{-1}	C_{3v}	D_0 ω/cm^{-1}	D_1 ω/cm^{-1}
a_2''	713.6i	117.9i	a_1	543.9	539.3
e″	915.3i	551.7	e	673.6	898.2
	745.0	1040.7i		902.7	679.7
a_2'	1111.4	1004.4	a_2	1048.4	1059.5
e′	938.3	1151.9	e	1157.6	1182.3
	1092.0	986.0		1662.6	1129.4
a_1'	1574.3	1574.3	a_1	1553.5	1553.4
e′	3311.4	3317.4	e	3363.5	3391.4
	3316.4	3310.3		3386.3	3360.1
a_1'	3519.0	3519.0	a_1	3445.7	3444.1

[a] $i = \sqrt{-1}$.

Table 5 Projected state-averaged harmonic vibrational frequencies for the cyclobutadienyl radical cation at the D_{4h} minimum on the E $\oplus$ ($b_1 \otimes b_2$) Jahn–Teller seam

Non-Abelian symmetry (D_{4h})	D_0 ω/ cm^{-1}	Symmetry (Abelian subgroup-D_{2h})	D_1 ω/ cm^{-1}	Symmetry (Abelian subgroup-D_{2h})	Δ/ cm^{-1}
Non-degenerate modes					
b_{2u}	123	b_{1u}	123	b_{1u}	0
a_{2u}	750	b_{1u}	750	b_{1u}	0
b_{2u}	936	b_{1u}	936	b_{1u}	0
b_{2g}	1134	b_{1g}	1134	b_{1g}	0
a_{2g}	1359	b_{1g}	1359	b_{1g}	0
a_{1g}	1360	a_g	1360	a_g	0
b_{1g}	2862	a_g	2862	a_g	0
a_{1g}	3418	a_g	3418	a_g	0
Degenerate modes					
e_g	741	b_{3g}	741	b_{2g}	362
	1103	b_{2g}	1103	b_{3g}	
e_u	937	b_{2u}	937	b_{3u}	186
	1123	b_{3u}	1123	b_{2u}	
e_u	1434	b_{2u}	1434	b_{3u}	101
	1535	b_{3u}	1535	b_{2u}	
e_u	3386	b_{2u}	3386	b_{3u}	27
	3413	b_{3u}	3413	b_{2u}	

does not have exact symmetry since the other mode is slightly mixed in.

Eqn. (36) allows the curvature of the seam to be determined. Let us illustrate this with respect to the out-of-plane e″ bending vibration. The first term in eqn. (36) is equal to the ratio of one component mode frequency to the frequency difference, and from Table 4 this can be calculated as 0.6015 (adopting a sign convention based upon which component mode is chosen *i.e.*, the mode we assign to state A or B). The second term is the ratio of the linear coupling constant for the gradient difference mode for one of the states ($\bar{Q}_{x_1}$) to the difference in the linear couplings for the $\bar{Q}_{x_1}$ mode. In the E $\otimes$ e Jahn–Teller case this will always be 0.5 since the coupling constants in eqn. (16) have equal magnitude but opposite sign; we must remember to keep track of the sign convention adopted previously. Taking the first component mode of the e'' pair as $\bar{Q}_i$ in eqn. (36) gives the following value for the seam curvature: $2(-0.6015 + 0.5) = -0.2030$. Thus if we follow the curvilinear combination of the bending mode and the gradient difference mode, we stay on the seam but lower the energy (see Fig. 12). Since the bending mode in question is doubly degenerate, the seam will lead to two distinct lower energy critical points. Overall, the D_{3h} point is a third-order saddle-point, when the a_2'' mode is also considered.

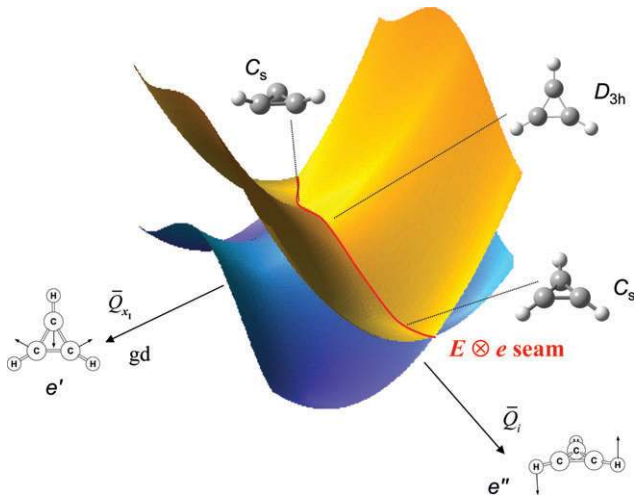

Fig. 12 Schematic of the seam of intersection in the C_3H_3 radical. The coordinates are the gradient difference (e′ in D_{3h} symmetry) and the symmetric out-of-plane bending vibration (a_2'' in D_{3h} symmetry). Both of these coordinates combine in a curvilinear manner to produce the seam shown in red.

The above example highlights the fact that the point around which the expansion of the potential energy is taken in eqns. (4) or (12) above must be carefully chosen. Clearly the global minimum on the E $\otimes$ e seam (Fig. 11a) is more suitable than the D_{3h} third-order saddle-point, even though the two points are only 10.80 kJ mol^{-1} apart. It would be interesting future work to compute the photoelectron and/or electron-attachment spectra of cyclopropenyl in detail to determine how the presence of lower-lying seam critical points affects the comparison to experiment.

Finally, the cyclopropenyl radical highlights an important aspect in multimode problems that has until now not been considered: namely that the 'obvious' Jahn–Teller point may not be the minimum on the seam. A schematic of the seam is shown in Fig. 12. We have shown that the symmetry is broken by some suitable (non-linear) combination of the gradient difference (gd) vector (one component of the first-order e′ pair), with either component of the degenerate (e″) out-of-plane vibration (Fig. 11) leading to a critical point on the seam of C_s symmetry. Thus, while the Jahn–Teller theorem predicts that separately each of these vibrations will lift the degeneracy, when combined *via* some suitable curvilinear transformation, the degeneracy is retained even though the (non-Abelian) symmetry is broken.

The E $\otimes$ ($b_1 \oplus b_2$) Jahn–Teller effect in the cyclobutadienyl radical cation

The cyclobutadienyl radical cation provides an example of the Jahn–Teller E $\otimes$ ($b_1 \oplus b_2$) effect. When a molecule contains a single C_4 axis of symmetry the gradient difference (eqn. (1)) and interstate coupling (eqn. (2)) vectors do not transform as a degenerate irrep of the point-group, but rather as different non-degenerate irreps. From this it follows that the gradients of the components of the degenerate electronic state (^1E_g) will be different (*i.e.*, the constant computed from eqn. (5) above is not equal to that computed from eqn. (6)).

To demonstrate some of the ideas discussed so far we will now focus our attention on the photoelectron spectrum of cyclobutadiene. This provides an example of computing the spectrum from wavepacket propagation. The object here is not to generate a high-quality photoelectron spectrum, but rather to show that using a very minimal model the qualitative features can be reproduced. We refer the reader to the body of work by Köppel *et al.*[50,66–68,90,91] for quantitative simulation of photoelectron spectra using wavepacket dynamics methods.

The ground state of cyclobutadiene (in D_{4h} symmetry) is $^1A_{1g}$ and therefore not subject to the Jahn–Teller effect. Cyclobutadiene is however subject to the related pseudo-Jahn–Teller (pJT) effect which we shall briefly discuss. The pJT effect is unfortunately sometimes called the second-order Jahn–Teller effect, but this is not 'second-order' as we use the term in this article. The pJT effect is due to a quadratic term in the interaction potential which lowers the molecular symmetry and increases the energy gap between two non-degenerate states.[92] However, the 'real' second-order (quadratic) Jahn–Teller effect is the lifting of a degeneracy at second-order in nuclear displacements (eqns. (4) and (12)). The pJT effect has been investigated in great detail[47,49,92–98] and used to explain such low-symmetry phenomena as solid-state structural distortions,[95] molecular fluxionality[96] and the preference for low coordination numbers to the right of the d-block.[97] The pJT

effect is the distortion of a high symmetry non-degenerate species to a lower symmetry geometry along a single non-totally symmetric vibrational coordinate. An energy stabilization occurs due to a mixing of the ground and excited states along this vibrational coordinate. Geometries subject to pJT distortion are saddle-points on the potential energy surface, rather than minima. Our group has recently proposed a test for pJT activity based on symmetry restrictions to the Hessian.[92] If the Hessian is computed using only configuration state functions (CSFs) of the appropriate symmetry for the electronic state then all eigenvalues are real at the pJT point. On the other hand, if all CSFs are included in the Hessian computation then one imaginary eigenvalue will appear (corresponding to the non-totally symmetric pJT active coordinate). This is because interstate coupling contributions to the Hessian mix the states; these are not present in symmetry-restricted computations.

In cyclobutadiene, the symmetry restricted frequency computation (*i.e.*, using only CSFs of A_{1g} symmetry) at the D_{4h} optimized geometry gives the lowest frequency mode as 507 cm^{-1} (having a_{2u} symmetry). When all CSFs are included in the frequency computation an imaginary frequency of 1448 cm^{-1} appears (see Fig. 13). The corresponding eigenvector has b_{2g} symmetry and leads to a rectangular geometry. The fact that the rectangular geometry is a minimum was also verified by a frequency computation using all CSFs. The pJT stabilization from the square-planar to rectangular geometry is 0.641 eV.

To test the reliability of our SA-CASSCF calculations for cyclobutadiene, the photoelectron spectrum was computed from a model Hamiltonian (using the potential from eqn. (20)). If the Franck–Condon (FC) point for ionization is on the conical intersection seam of the ion, as often is the case for Jahn–Teller problems, then the important linear modes are the gradient difference and interstate coupling (lifting the degeneracy at first-order). However, totally symmetric modes, which cannot lift the degeneracy at any order, can be important to obtain the correct vibrational structure in the spectrum when this is not the case. The C_4H_4 seam minimum is at symmetrical D_{4h} geometries and our computations show that this seam does not extend to lower symmetry structures as in the previous C_3H_3 example. Thus, the minimum on the seam is displaced from the ionization FC point and it is important to include at least one totally symmetric mode in the model Hamiltonian. For a discussion of the inclusion of totally symmetric modes see ref. 99.

The model Hamiltonian included three modes: one totally symmetric mode with frequency 1516 cm^{-1}, in addition to the gradient difference and interstate coupling modes. This frequency is taken from the D_{2h} ground state minimum. The force

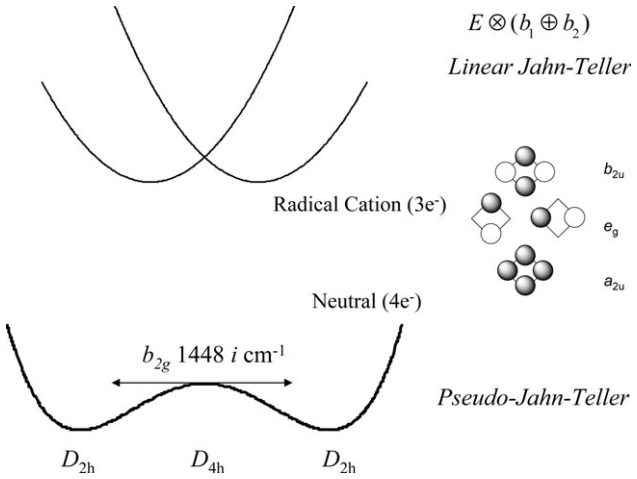

Fig. 13 Schematic potential surfaces for neutral C_4H_4 (subject to a pseudo-Jahn–Teller distortion) and the photoionised radical cation (subject to a linear E $\otimes$ (b_1 $\oplus$ b_2) effect). The π-orbitals involved are shown to the right, labelled in D_{4h} symmetry.

Table 6 Parameters used in the linear vibronic coupling model to simulate the photoelectron spectrum of cyclobutadiene. The coordinates used were mass-frequency scaled normal modes with the D_{4h} minimum energy conical intersection point as the reference geometry. In these coordinates, the D_{2h} Franck–Condon point is at −1.86, −1.86, 0.68 along the gradient difference and interstate coupling vectors, and the totally-symmetric vibration respectively

Linear coupling along $\bar{Q}_{x_1}$	0.184 eV
Linear coupling along $\bar{Q}_{x_2}$	0.240 eV
Harmonic vibrational frequency for $\bar{Q}_{x_1}$ [a]	983.99 cm^{-1}
Harmonic vibrational frequency for $\bar{Q}_{x_2}$ [a]	959.80 cm^{-1}
Harmonic vibrational frequency for A_g mode[a]	1516.31 cm^{-1}
ΔE (neutral − radical cation)	7.65 eV[b]
	8.10 eV[c]

[a] Taken from the neutral D_{2h} minimum. [b] SA-CASSCF/cc-pVDZ [c] Experimental value taken from ref. 32.

at the Franck–Condon geometry along this mode was then calculated to provide the relevant linear parameter and this was combined with the linear parameters for the branching space modes to give the full Hamiltonian. The parameters used are collected in Table 6.

The photoelectron spectrum was obtained as the Fourier transform of the autocorrelation function obtained from a wavepacket propagation over 150 fs using the Heidelberg MCTDH package.[100] It is shown in Fig. 14. For more details about the MCTDH method, including further examples of the computation of photoelectron spectra of Jahn–Teller active molecules see refs. 99 and 101 and references therein. A good qualitative agreement with experiment[32] is obtained using only the parameters given in Table 6, which indicates that all the

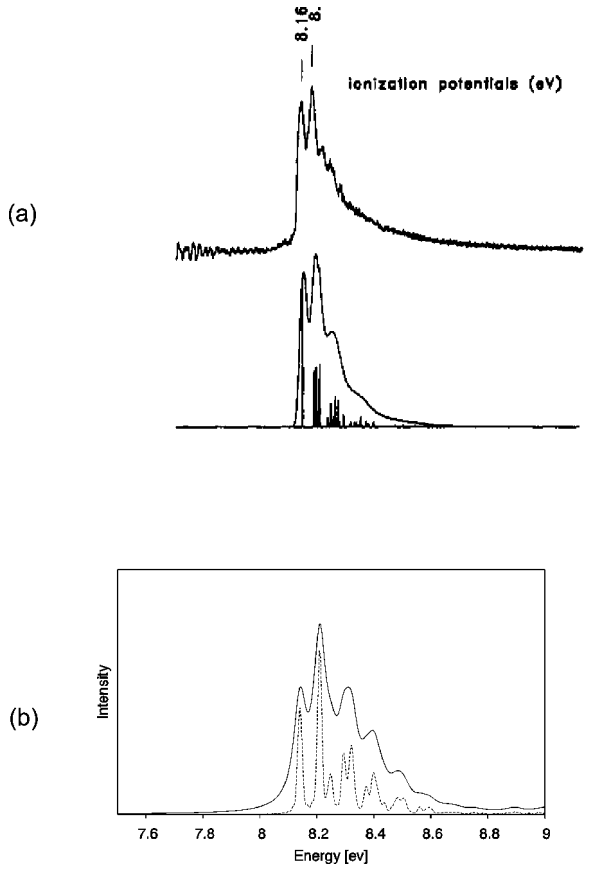

Fig. 14 (a) Experimental (taken from ref. 32 with permission) and (b) computed photoelectron spectrum for $C_4H_4^+$. Simulated spectrum computed using the gradient difference, interstate coupling and a totally symmetric mode. All parameters in the linear model Hamiltonian were calculated using SA-CASSCF. The spectral envelope includes a phenomenological broadening to match the experiment.

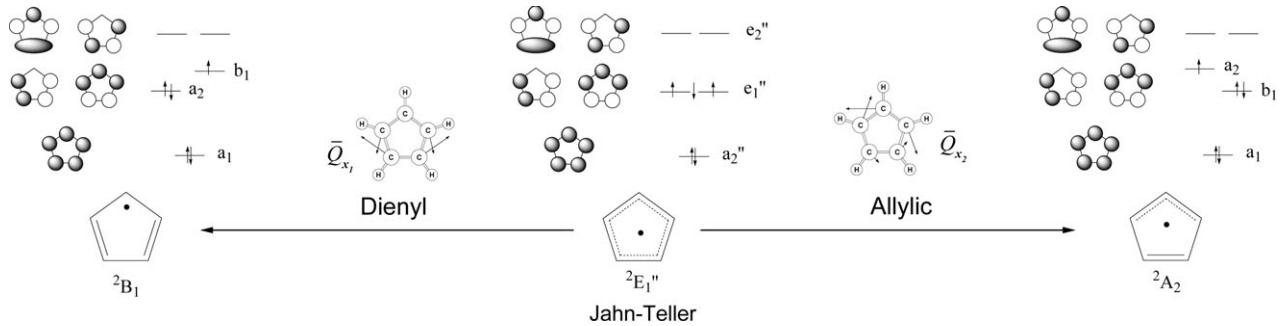

Fig. 15 The Jahn–Teller effect for the Cp radical (D_{5h}). Distortion along the gradient difference vector ($\bar{Q}_{x_1}$) (a_1 symmetry in C_{2v} subgroup) leads to a dienylic species, while distortion along the interstate coupling vector ($\bar{Q}_{x_2}$) (b_2 symmetry in C_{2v} subgroup) leads to an allylic species.

important vibronic coupling data needed to reproduce the first photoelectron band can be obtained from the SA-CASSCF frequency analysis (Fig. 14). It should be noted that the second-order terms would merely broaden the spectra since in this particular example the first-order and second-order effects are rigorously separable due to the symmetry of the Hamiltonian.

The Jahn–Teller effect in Cp

The cyclopentadienyl radical has a degenerate ground state at D_{5h} geometries ($^2E_1''$), which is subject to a Jahn–Teller distortion.[23,24,102] The D_{5h} symmetry is broken by the Jahn–Teller distortion and the $^2E_1''$ electronic state is split into two different states which transform as $^2A_2$ and $^2B_1$ in the C_{2v} subgroup. These two states can be classified as a dienyl state ($^2B_1$) and an allyl state ($^2A_2$): see Fig. 15 for a VB representation of the states and the Jahn–Teller distortion which lifts the degeneracy at first-order.

The modes which lift the degeneracy at first-order have e_2' symmetry. Thus, the interstate coupling and gradient difference vectors transform as e_2'. The gradient difference vector is totally symmetric in the C_{2v} subgroup and corresponds to the dienyl distortion, while the interstate coupling vector transforms as b_2 in the C_{2v} subgroup and corresponds to the allyl distortion.

By projecting these modes from the Hessian we remove the components of the gradient along the three remaining normal modes of e_2' symmetry in the 'intersection space'. As discussed in the previous section (eqn. (11)) all linear coupling is now contained within the space spanned by the gradient difference and interstate coupling vectors *i.e.*, the branching space. For the other modes of e_2', the degeneracy is not lifted at first-order in our vibrational coordinate basis.

The results of the vibrational frequency analysis are presented in Table 7. It can be seen that the non-degenerate modes have the same frequency on each surface. For an E $\otimes$ e Jahn–Teller conical intersection, this is expected since non-degenerate modes do not lift the degeneracy at first or second-order *i.e.*, only two-component modes that together transform as a degenerate irreducible representation of the molecular point group can lift the degeneracy of the electronic state in an E $\otimes$ e Jahn–Teller system.

The modes which lift the degeneracy at second-order are of e_1' and e_1'' symmetry. The frequency splittings for these modes can be seen to be quite small (Table 7). The largest splitting of 87 cm^{-1} corresponds to an out-of-plane bending motion. This can be understood if one considers the valence bond resonance structures. For example, there will be less resistance to the b_2 component vibration for the allylic state; therefore the frequency will be lower. The splitting is relatively small though. This is in agreement with findings of Applegate, Miller and Barckholtz,[23] who find that all the second-order couplings in Cp are quite small in magnitude.

Modes ν_{10} and ν_{13} show a small splitting (Table 7). This requires some further comment. These modes are of e_2'' symmetry and the quadratic coupling constant between components of these vibrations is zero by symmetry. The only way the degeneracy can be lifted at second-order along these modes is by invoking a cross-quadratic term, which is normally neglected. The cross-quadratic coupling can take place *via* the coupling of components of modes of e_1'' symmetry with those of e_2'' symmetry.[23] Note that the components of these degenerate vibrations transform as the same irreps in the C_{2v} subgroup (Table 7). Within our computations splittings of this type can occur since there are no symmetry restrictions placed upon the calculation of the state-averaged Hessian. The value of the splitting in both of these modes is 7 cm^{-1}. Since there is only one mode of e_1'' symmetry, only this mode can be responsible for the splitting, explaining why the 7 cm^{-1} splitting is the same for both modes. This also explains why the splitting in the E_1'' mode is large compared to the other modes, since it will also show this effect with both modes of e_2'' symmetry. Within our vibrational coordinate basis (eqn. (11)), the modes ν_{10}, ν_{12} and ν_{13} show an effective splitting due to the terms in eqns. (8)–(10), which are second-order intra- and interstate couplings.

Table 7 Projected state-averaged harmonic vibrational frequencies for both components of the degenerate $^1E_1''$ state of cyclopentadienyl (Cp)

Mode	Non-Abelian symmetry (D_{5h})	D_0 ω/ cm^{-1}	Symmetry (Abelian subgroup-C_{2v})	D_1 ω/ cm^{-1}	Symmetry (Abelian subgroup-C_{2v})	Δ/ cm^{-1}
Non-degenerate modes						
ν_{11}	a_2''	687	b_2	687	b_2	0
ν_5	a_1'	1172	a_1	1172	a_1	0
ν_6	a'_2	1388	b_1	1388	b_1	0
ν_1	a'_1	3408	a_1	3408	a_1	0
Degenerate modes						
ν_{10}	e_2''	529	b_2	536	b_2	7
		548	a_2	540	a_2	
ν_{12}	e_1''	690	b_2	690	a_2	87
		777	a_2	777	b_2	
ν_{13}	e_2''	867	b_2	860	a_2	7
		868	a_2	874	b_2	
ν_9	e_2'	919	a_1	919	a_1	0
		919	b_1	919	b_1	
ν_8	e_1'	1059	a_1	1059	b_1	9
		1068	b_1	1068	a_1	
ν_7	e_2'	1232	b_1	1232	b_1	0
		1232	a_1	1232	a_1	
ν_4	e_2'	1539	b_1	1539	a_1	12
		1551	a_1	1551	b_1	
ν_3	e_2'	3373	a_1	3373	a_1	0
		3373	b_1	3373	b_1	
ν_2	e_2'	3391	a_1	3391	b_1	1
		3392	b_1	3392	a_1	

Conclusions

In this perspective we have shown how one can obtain second-order degeneracy splittings at a conical intersection. This is based on the projection of the 'branching space' from the state-averaged nuclear Hessian for each component of the degenerate electronic state, and the second-order effects are obtained as the differences in the eigenvalues. The corresponding eigenvectors define a set of rectilinear vibrational coordinates, which form a representation of the $(3N-8)$-dimensional 'intersection space'. The potential surfaces along these coordinates show analogous topologies to the well-known Renner–Teller topologies of linear molecules with non-zero electronic angular momentum.

The seam of intersection is a hypercurve and a second-order approximation to it can be obtained using both the 'branching space' and the 'intersection space'. A curvilinear transformation of the two sets of coordinates provides a representation of the seam to second-order, *i.e.*, for small finite displacements along the hypercurve. Using the second-derivative of the electronic potential energy with respect to the curvilinear seam allows us to characterise optimised points on the seam as minima or saddle-points. Our analysis shows (*e.g.* for the cyclopropenyl radical) that a Jahn–Teller geometry may not be a minimum on the seam. Thus, even at a Jahn–Teller point the symmetry may be lowered while the degeneracy is retained.

It has recently become apparent that, for photochemical problems in which the reaction path does not lie within the 'branching space', segments of the seam of intersection need to be mapped out.[14,16] This is because higher energy domains on the seam can provide different points for radiationless decay and a variety of photoproducts may result. For example, see ref. 14 where direct dynamics has been used to elucidate the mechanism of photochromism in diarylethylenes, which involves decay at various points on the seam of intersection away from its minimum. In the future, we expect our methodology to be used to characterise and map out important segments of the intersection seam.

Returning to Jahn–Teller symmetry imposed conical intersections: when the Jahn–Teller geometry is a minimum on the seam, the original rectilinear 'branching space' and 'intersection space' coordinates can be used to define an alternative vibrational coordinate basis set to simulate vibronic spectra, using either wavepacket dynamics or by diagonalizing a model vibronic Hamiltonian. Our method for obtaining the potential constants which would be necessary in either case is very similar to that of Miller *et al.*[23,26–28] One advantage our method has is that the Jahn–Teller surfaces are all computed at the same level of theory, based around a Taylor expansion at the conical intersection. This is in contrast to the Barckholtz–Miller model in which a (fictitious) average potential is used to obtain the second-order potential constants in the expansion. Future work will include the computation of Jahn–Teller spectra on some well-studied molecules (*e.g.*, the methoxy radical and the benzene radical cation) in order to parameterise a model Hamiltonian in a more systematic manner, and to further decompose each contribution from the state-averaged Hessian, so that more terms may included (*e.g.*, all second-order interstate coupling).

It should also be straightforward to extend the above methodology to higher degeneracies in the cubic or icosahedral point groups. For example the von Neumann–Wigner theorem states that the 'branching space' for a triply degenerate state will be five-dimensional. This corresponds to the $T \otimes (t_2 \oplus e)$ Jahn–Teller effect. In principle our method could be extended to such cases. Recent studies have shown the possible importance of triply-degenerate states in general.[103,104]

Many photochemical reaction mechanisms are now known to involve reaction paths *via* conical intersections. The main spectroscopic technique used has been time-resolved pump–probe spectroscopy, on the picosecond to femtosecond timescale. It is not yet possible to obtain 'static' high-resolution electronic spectra and hence detailed vibrational structure in the region of the conical intersections that typically occur in photochemical reactivity problems, as the molecules are not in the crossing region for long enough. However, for the specialised case of a Jahn–Teller crossing, high resolution spectra can often be obtained, yielding detailed information concerning the intersecting potential energy surfaces which can in turn be used to fit the experimental spectrum. Here, theory and experiment can be compared and calibrated directly,[105] in contrast to a typical photochemical reaction. However, this distinction is not fundamentally between 'photochemistry' and 'Jahn–Teller spectroscopy', but has to do with whether the molecule is constantly in the vicinity of the crossing (often the case for Jahn–Teller systems), or whether the crossing is encountered briefly along a reaction path leading elsewhere (often the case photochemically).

We have recently shown[14] that an extended seam away from the crossing minimum is important for photochemistry. In this article, we report that for a simple Jahn–Teller system (cyclopropenyl, C_3H_3), there is also an extended crossing seam, and there must be many other Jahn–Teller systems for which this occurs. Studying model Jahn–Teller systems can therefore help in understanding the nature of the extended seam now recognised as important for photochemistry. Moreover, greater interaction between experimental and theoretical groups studying photochemical mechanisms and Jahn–Teller spectroscopy would be beneficial, as each can generate complementary insights into surface crossings. As has been pointed out elsewhere recently,[106] there is still a 'strange orthogonality between the conical intersection and Jahn–Teller communities'.

Appendix: Group theoretical considerations

An understanding of the symmetries of the modes inducing a first- and/or second-order Jahn–Teller effect often reduces the complexity of eqn. (4), since only certain modes can give non-zero potential constants (eqns. (5)–(10)). In this appendix we shall expand on some of the group theoretical ideas using the examples discussed above.

Let us begin with pseudo-Jahn–Teller (pJT) effect as discussed for the C_4H_4 radical cation. The pJT effect is based on the Herzberg–Teller expansion of the electronic energy,[62]

$$E = E_0 + \left\langle \Psi_0 \left| \frac{\partial V}{\partial Q} \right| \Psi_0 \right\rangle + \frac{Q^2}{2} \left\langle \Psi_0 \left| \frac{\partial^2 V}{\partial Q^2} \right| \Psi_0 \right\rangle + \sum_i \frac{\left[\left\langle \Psi_0 \left| \frac{\partial V}{\partial Q} \right| \Psi_i \right\rangle \right]^2}{(E_0 - E_i)} \quad (45)$$

where Ψ_0 is the electronic ground state wavefunction, Ψ_i are excited electronic wavefunctions, V is the potential energy and Q is a normal coordinate obtained at a critical point on the non-degenerate potential surface. Since the expansion is at a critical point only the last term survives. In order for this term to be non-zero the direct product of the irreducible representations labelling the electronic states must be equal to that of the vibrational normal coordinate, *i.e.*,

$$\Gamma_0 \otimes \Gamma_i = \Gamma_Q \quad (46)$$

Thus for C_4H_4 at D_{4h} geometries any b_{2g} vibration can lower the ground state energy by allowing the ground ($^1A_{1g}$) and excited ($^1B_{2g}$) states to mix. Of course the pJT interaction is governed by the energy difference in the denominator of eqn. (45), which is of course not true for actual conical intersection geometries where the energy gap is exactly zero and the geometry is not a critical point on the potential energy surface.

We now consider the case of an accidental intersection (between states Ψ_n and Ψ_m) in an Abelian point-group. For a

first-order potential constant (eqn. (5)–(7)) to be non-vanishing, the condition is that the direct product of the irreps labeling the electronic states and the irrep labeling the vibrational coordinate $\bar{Q}$ should contain the totally symmetric irrep (Γ_A).[50,99]

$$\Gamma_n \otimes \Gamma_m \otimes \Gamma_{\bar{Q}} \supset \Gamma_A \quad (47)$$

Obviously the intrastate couplings (eqns. (5) and (6)) can only be non-zero for the totally symmetric modes. Furthermore in our vibrational coordinate basis (eqn. (11)) the only non-zero first-order term is the one involving the gradient difference vector ($\bar{Q}_{x_1}$). For the off-diagonal interstate coupling terms (eqn. (7)) the symmetry of the vibrational coordinates $\bar{Q}_i$ is therefore determined by the direct product of the irreps of the electronic states, *e.g.*, in the C_{2v} point group if the states have A_2 and B_1 symmetry then only modes of $A_2 \otimes B_1 = B_2$ symmetry have non-zero interstate coupling terms. In the vibrational coordinate basis of eqn. (11) this reduces to only the interstate coupling vector, and the potential constant (eqn. (7)) is the length of this vector.

In the Jahn–Teller effect the direct products in eqn. (47) now involve degenerate point-groups, and as a result the symmetries of the Jahn–Teller active modes are taken as the symmetrized direct product of the electronic state irrep with itself.[107] In non-cubic point groups this leads to the well-known $E \otimes e$ and $E \otimes (b_1 \oplus b_2)$ cases.[47–50]

Similar to the linear Jahn–Teller coupling, the possibility of quadratic coupling can be evaluated group theoretically.[26] For specific point-groups the symmetries of first- and second-order Jahn–Teller modes may be determined;[26] the number of such modes of course being determined by the symmetry-adapted vibrational coordinates of the particular molecule. For a vibrational coordinate to lift the degeneracy at second-order the symmetrized square of the direct product of the irrep of the state with itself must contain that of the direct product of the (appropriately symmetrized) irrep of the two vibrational coordinates.

$$[\Gamma_E \otimes \Gamma_E] = [\Gamma_{\bar{Q}_i} \otimes \Gamma_{\bar{Q}_j}] \quad (48)$$

where Γ_E is the irrep of the electronic state, and $\Gamma_{\bar{Q}_i}$, $\Gamma_{\bar{Q}_j}$ are the irreps of the vibrational coordinates. For example in the C_4H_4 radical cation, the molecular point-group is D_{4h}. The electronic state is ^1E_g, thus the linear Jahn–Teller active coordinates span $[E_g \otimes E_g] = b_{1g} \oplus b_{2g}$. The direct product of the quadratically active coordinates must therefore also span $b_{1g} \oplus b_{2g}$. In the D_{4h} point-group both degenerate irreps have the desired direct products since $[E_g \otimes E_g] = b_{1g} \oplus b_{2g}$ and also $[E_u \otimes E_u] = b_{1g} \oplus b_{2g}$. However there can be no cross-quadratic coupling since $[E_g \otimes E_u] = b_{1u} \oplus b_{2u}$. For evaluating whether certain cross-quadratic couplings are possible it is often easier to use an Abelian subgroup. As another example, the cyclopentadienyl radical (Cp) has a degenerate electronic $^2E_1''$ ground state at D_{5h} geometries.[23,24,102] The modes which lift the degeneracy at first-order are of e_2' symmetry, while the modes that lift the degeneracy at second-order are of e_1'' or e_1'' symmetry. It is also possible that the degeneracy can be lifted at second-order, by coupling the components of modes of e_1'' and e_2'' symmetry. In the C_{2v} subgroup of D_{5h}, both the E_1'' and E_2'' irreps are decomposed to $A_2 \oplus B_2$. Therefore cross-quadratic coupling can occur between both component modes with the same subgroup symmetry. For the general set of vibrational coordinates Q_i (in eqn. (4)), all modes of e_2' symmetry can lift the degeneracy at first-order (*i.e.*, there is a non-zero κ_i for all modes with this symmetry). There are four modes of this symmetry for Cp. Thus the coupling κ_i is spread over all these modes (see discussion in Barkholtz and Miller[23,26,28]). Our alternative set of vibrational coordinates, where the degeneracy is lifted at first-order only in the branching space, simplifies eqn. (4) and allows a separation of those modes that lift the degeneracy at first-order from the rest of the space.

Acknowledgements

All computations were carried out on an IBM-SP2 funded jointly by IBM-UK and HEFCE (UK). L. Blancafort is financed by the Ramón y Cajal programme from the Spanish Ministerio de Ciencia y Tecnología and by Grants No. BQU200204112-C02-02 and BZ2002–03334 from the Spanish Dirección General de Enseñanza Superior e Investigación Científica y Técnica (MECD).

References

1 T. Tahara, in *Advances in Multi-photon Processes and Spectroscopy*, ed. S. H. Lin, A. A. Villaeys, and Y. Fujimura, World Scientific, Singapore, 2004.
2 A. H. Zewail, *J. Phys. Chem. A*, 2000, **104**, 5660.
3 A. H. Zewail, *J. Phys. Chem.*, 1996, **100**, 12701.
4 A. H. Zewail, *J. Phys. Chem.*, 1993, **97**, 12427.
5 S. A. Trushin, W. Fuß and W. E. Schmid, *Chem. Phys.*, 2000, **259**, 313.
6 C. E. Crespo-Hernández, B. Cohen, P. M. Hare and B. Kohler, *Chem. Rev.*, 2004, **104**, 1977.
7 *Femtochemistry and Femtobiology*, ed. A. Douhal and J. Santamaria, World Scientific, Singapore, 2002.
8 A. Stolow, A. E. Bragg and D. M. Neumann, *Chem. Rev.*, 2004, **104**, 1719.
9 F. Bernardi, M. Olivucci and M. A. Robb, *Chem. Soc. Rev.*, 1996, **25**, 321.
10 M. Olivucci and A. Migani, in *Conical Intersections: Electronic Structure, Dynamics and Spectroscopy*, ed. W. Domcke, D. Yarkony and H. Köppel, World Scientific, Singapore, 2004.
11 M. A. Robb, M. Garavelli, M. Olivucci and F. Bernardi, in *A Computational Strategy for Organic Photochemistry*, ed. K. B. Lipkowitz and D. B. Boyd, Wiley-VCH, New York, 2000.
12 M. J. Bearpark, F. Bernardi, M. Olivucci, M. A. Robb and B. R. Smith, *J. Am. Chem. Soc.*, 1996, **118**, 5254.
13 L. Blancafort, D. Gonzalez, M. Olivucci and M. A. Robb, *J. Am. Chem. Soc.*, 2002, **124**, 6398.
14 M. Boggio-Pasqua, M. Ravaglia, M. J. Bearpark, M. Garavelli and M. A. Robb, *J. Phys. Chem. A*, 2003, **107**, 11139.
15 N. Ismail, L. Blancafort, M. Olivucci, B. Kohler and M. A. Robb, *J. Am. Chem. Soc.*, 2002, **124**, 6818.
16 A. Migani, M. A. Robb and M. Olivucci, *J. Am. Chem. Soc.*, 2003, **125**, 2804.
17 M. Olivucci, I. N. Ragazos, F. Bernardi and M. A. Robb, *J. Am. Chem. Soc.*, 1993, **115**, 3710.
18 I. J. Palmer, I. N. Ragazos, M. A. Robb, F. Bernardi and M. Olivucci, *J. Am. Chem. Soc.*, 1993, **115**, 673.
19 M. J. Paterson, P. A. Hunt, M. A. Robb and O. Takahashi, *J. Phys. Chem. A*, 2002, **106**, 10494.
20 M. J. Paterson, L. Blancafort, S. Wilsey and M. A. Robb, *J. Phys. Chem. A*, 2002, **106**, 11431.
21 M. J. Paterson, M. A. Robb, L. Blancafort and A. De Bellis, *J. Am. Chem. Soc.*, 2004, **126**, 2912.
22 A. Sanchez-Galvez, P. A. Hunt, M. A. Robb, M. Olivucci, T. Vreven and H. B. Schlegel, *J. Am. Chem. Soc.*, 2000, **122**, 2911.
23 B. E. Applegate, T. A. Miller and T. A. Barckholtz, *J. Chem. Phys.*, 2001, **114**, 4855.
24 B. E. Applegate, A. J. Bezant and T. A. Miller, *J. Chem. Phys.*, 2001, **114**, 4869.
25 B. E. Applegate and T. A. Miller, *J. Chem. Phys.*, 2002, **117**, 10654.
26 T. A. Barckholtz and T. A. Miller, *Int. Rev. Phys. Chem.*, 1998, **17**, 435.
27 T. A. Barckholtz, M. C. Yang and T. A. Miller, *Mol. Phys.*, 1999, **97**, 239.
28 T. A. Barckholtz and T. A. Miller, *J. Phys. Chem. A*, 1999, **103**, 2321.
29 T. A. Miller and V. E. Bondybey, in *Molecular Ions: Spectroscopy, Structure and Chemistry*, ed. T. A. Miller and V. E. Bondybey, North-Holland, New York, 1983.
30 C.-Y. Ng, *Annu. Rev. Phys. Chem.*, 2002, **53**, 101.
31 S. E. Canton, A. J. Yencha, E. Kukk, J. D. Bozek, M. C. A. Lopes, G. Snell and N. Berrah, *Phys. Rev. Lett.*, 2002, **89**, 45502.
32 D. W. Kohn and P. Chen, *J. Am. Chem. Soc.*, 1993, **115**, 2844.
33 R. Lindner, H. Sekiya and H. Müller-Dethlefs, *Angew. Chem. Int. Ed. Engl.*, 1993, **32**, 1364.
34 L.-S. Wang, B. Niu, Y. T. Lee, D. A. Shirley, E. Ghelichkhani and E. R. Grant, *J. Chem. Phys.*, 1990, **93**, 6318.

35 T. A. Miller, B. R. Zegarski, T. J. Sears and V. E. Bondybey, *J. Phys. Chem.*, 1980, **84**, 173.
36 T. J. Sears, T. A. Miller and V. E. Bondybey, *J. Am. Chem. Soc.*, 1980, **102**, 4864.
37 T. J. Sears, T. A. Miller and V. E. Bondybey, *J. Am. Chem. Soc.*, 1981, **103**, 326.
38 T. J. Sears, T. A. Miller and V. E. Bondybey, *J. Chem. Soc., Faraday Discuss.*, 1981, **71**, 175.
39 M. C. Heaven and T. A. Miller, in *Laser Induced Photochemistry in a Supersonic Expansion*, Howard University Press, Washington, DC, 1985.
40 A. Geers, J. Kappert, F. Temps and T. J. Sears, *J. Chem. Phys.*, 1993, **98**, 4297.
41 M. J. Paterson, L. Blancafort, M. J. Bearpark and M. A. Robb, *J. Chem. Phys.*, 2004, **121**, 11562.
42 O. Weingart, A. Migani, M. Olivucci, M. A. Robb, V. Buss and P. Hunt, *J. Phys. Chem. A*, 2004, **108**, 4685.
43 J. von Neumann and E. Wigner, *Z. Phys.*, 1929, **30**, 467.
44 *Quantum Chemistry: Classic Scientific Papers*, ed. H. Hettema, World Scientific, Singapore, 2000.
45 D. R. Yarkony, *J. Phys. Chem. A*, 2001, **105**, 6277.
46 T. A. Jahn and E. Teller, *Proc. R. Soc. London, Ser. A*, 1937, **161**, 220.
47 I. B. Bersuker and V. Polinger, *Vibronic Interactions in Molecules and Crystals*, Springer-Verlag, Berlin, 1989.
48 R. Englman, *The Jahn–Teller Effect in Molecules and Crystals*, Wiley, New York, 1972.
49 I. B. Bersuker, *Chem. Rev.*, 2001, **101**, 1067.
50 H. Köppel, W. Domcke and L. S. Cederbaum, *Adv. Chem. Phys.*, 1984, **57**, 59.
51 M. S. Child, *Mol. Phys.*, 1960, **3**, 601.
52 D. R. Yarkony, *Acc. Chem. Res.*, 1998, **31**, 511.
53 D. R. Yarkony, *Rev. Mod. Phys.*, 1996, **68**, 985.
54 E. Teller, *J. Phys. Chem.*, 1937, **41**, 109.
55 E. Teller, *Isr. J. Chem.*, 1969, **7**, 227.
56 M. J. Bearpark, M. A. Robb and H. B. Schlegel, *Chem. Phys. Lett.*, 1994, **223**, 269.
57 I. N. Ragazos, M. A. Robb, F. Bernardi and M. Olivucci, *Chem. Phys. Lett.*, 1992, **197**, 217.
58 D. R. Yarkony, *J. Phys. Chem. A*, 2004, **108**, 3200.
59 R. F. Frey and E. R. Davidson, in *Advances in Electronic Structure Theory: Calculation and Characterisation of Potential Energy Surfaces*, Wiley, New York, 1990.
60 G. J. X. Atchity, S. S. Xantheas and K. Ruedenberg, *J. Chem. Phys.*, 1991, **95**, 1862.
61 E. Renner, *Z. Phys.*, 1934, **92**, 172.
62 G. Herzberg, *Electronic Spectra and Electronic Structure of Polyatomic Molecules*, Van Nostrand, Toronto, ON, 1966.
63 T. J. Lee, D. J. Fox, H. F. Schaeffer III and R. M. Pitzer, *J. Chem. Phys.*, 1984, **81**, 356.
64 S. Matsika and D. Yarkony, *J. Phys. Chem. A*, 2002, **106**, 2580.
65 L. S. Cederbaum, H. Koppel and W. Domcke, *Int. J. Quantum Chem.*, 1981, **251**.
66 M. Döscher, H. Köppel and P. G. Szalay, *J. Chem. Phys.*, 2002, **117**, 2645.
67 J. Schmidt-Klügmann, H. Köppel, S. Schmatz and P. Botschwina, *Chem. Phys. Lett.*, 2003, **369**, 21.
68 H. Köppel, L. S. Cederbaum and W. Domcke, *J. Chem. Phys.*, 1988, **89**, 2023.
69 E. B. Wilson, Jr, J. C. Decius and P. C. Cross, *Molecular Vibrations: The Theory of Infrared and Raman Spectras*, Dover, New York, 1980.
70 P. W. Atkins and R. S. Friedman, *Molecular Quantum Mechanics*, Oxford University Press, New York, 3rd edn., 1997.
71 D. R. Yarkony, *J. Chem. Phys.*, 2000, **112**, 2111.
72 E. Haller, H. Köppel, L. S. Cederbaum, W. von Niessen and G. Bieri, *J. Chem. Phys.*, 1983, **78**, 1359.
73 J. Eiding, R. Schneider, W. Domcke, H. Köppel and W. von Niessen, *Chem. Phys. Lett.*, 1991, **177**, 345.
74 S. Mahaptra, V. Vallet, C. Woywood, H. Köppel and W. Domcke, *Chem. Phys.*, 2004, **304**, 17.
75 C. C. Chancey and M. C. M. O' Brien, *The Jahn–Teller Effect in C_{60} and Other Icosohedral Complexes*, Princeton University Press, Princeton, NJ, 1997.
76 P. W. Atkins, M. S. Child and C. S. G. Phillips, *Tables for Group Theory*, Oxford University Press, Oxford, 1970.
77 U. Höper, P. Botschwina and H. Köppel, *J. Chem. Phys.*, 2000, **112**, 4132.
78 C. Cossart-Magos and S. Leach, *Chem. Phys.*, 1980, **48**, 349.
79 A. G. Baboul and H. B. Schlegel, *J. Chem. Phys.*, 1997, **107**, 9413.
80 M. J. Frisch, G. W. Trucks, H. B. Schlegel, G. E. Scuseria, M. A. Robb, J. R. Cheeseman, V. G. Zakrzewski, J. A. Montgomery, R. E. Stratmann, J. C. Burant, S. Dapprich, J. M. Millam, A. D. Daniels, K. N. Kudin, M. C. Strain, O. Farkas, J. Tomasi, V. Barone, M. Cossi, R. Cammi, B. Mennucci, C. Pomelli, C. Adamo, S. Clifford, J. Ochterski, G. A. Petersson, P. Y. Ayala, Q. Cui, K. Morokuma, D. K. Malick, A. D. Rabuck, K. Raghavachari, J. B. Foresman, J. Cioslowski, J. V. Ortiz, B. B. Stefanov, G. Liu, A. Liashenko, P. Piskorz, I. Komaromi, R. Gomperts, R. L. Martin, D. J. Fox, T. Keith, M. A. Al-Laham, C. Y. Peng, A. Nanayakkara, C. Gonzalez, M. Challacombe, P. M. W. Gill, B. G. Johnson, W. Chen, M. W. Wong, J. L. Andres, M. Head-Gordon, E. S. Replogle and J. A. Pople, *GAUSSIAN 99 (Revision C1)*, Gaussian, Inc., Pittsburgh, PA, 1999.
81 J. W. Ochterski, *Vibrational Analysis in Gaussian*, 1999, available at http://www.gaussian.com/g_whitepap/vib.htm.
82 T. Vreven, *The Theoretical Investigation of Photochemical Reactions. Ab initio Trajectories with Surface Hopping*, PhD Thesis, University of London, 1998.
83 G. Fischer, *Vibronic Coupling: The Interaction Between the Electronic and Nuclear Motions*, Academic Press, London, 1984.
84 Note about terminology: We shall refer to a vibrational mode as degenerate if there are two component modes which together transform as a degenerate irreducible representation of the point group, although it should be remembered that the vibrational frequency of each component mode is different.
85 Here we only use three unique Renner–Teller topologies (see Fig. 1). The other two Renner–Teller topologies (types II and V in the original nomenclature) refer to quartic splitting of the potentials in *e.g.*, Δ states of linear molecules. We shall not consider those here. Thus, our type-II corresponds to type-III and our type-III corresponds to the type-IV, in the nomenclature of ref. 63.
86 M. Peric, C. M. Marian and S. D. Peyerimhoff, *J. Chem. Phys.*, 2001, **114**, 6086.
87 M. Peric, L. Stevanovic and S. Jerosimic, *J. Chem. Phys.*, 2002, **117**, 4233.
88 We use vibrational frequencies in cm^{-1} in the tables to give some idea of the curvature, but use force constants (not mass-weighted) in the equations.
89 S.-G. He and D. J. Clouthier, *J. Chem. Phys.*, 2004, **120**, 8544.
90 H. Köppel, W. Domcke and L. S. Cederbaum, *J. Chem. Phys.*, 1981, **74**, 2945.
91 H. Köppel, *Z. Phys. Chem.*, 1997, **200**, 3.
92 M. J. Bearpark, L. Blancafort and M. A. Robb, *Mol. Phys.*, 2002, **100**, 1735.
93 U. Öpik and M. H. L. Pryce, *Proc. R. Soc. London, Ser. A*, 1957, **238**, 425.
94 R. G. Pearson, *J. Am. Chem. Soc.*, 1969, **91**, 4947.
95 J. K. Burdett, *Molecular Shapes*, Wiley, New York, 1980.
96 I. B. Bersuker, *Electronic Structure and Properties of Transition Metal Compounds. Introduction to the Theory*, Wiley, New York, 1996.
97 B. N. Figgis and M. A. Hitchman, *Ligand Field Theory and its Applications*, Wiley-VCH, New York, 2000.
98 M. J. Paterson, N. P. Chatterton and G. S. McGrady, *New J. Chem.*, 2004, **28**, 1434.
99 G. A. Worth and L. S. Cederbaum, *Annu. Rev. Phys. Chem.*, 2004, **55**, 127.
100 G. A. Worth, M. H. Beck, A. Jäckle and H.-D. Meyer, *The MCTDH Package (version 8.2)*, University of Heidelberg, 2000.
101 H.-D. Meyer and G. A. Worth, *Theor. Chem. Acc.*, 2003, **109**, 251.
102 M. J. Bearpark, M. A. Robb and N. Yamamoto, *Spectrochim. Acta, Part A*, 1999, **55**, 639.
103 S. Han and D. R. Yarkony, *J. Chem. Phys.*, 2003, **119**, 11561.
104 L. Blancafort and M. A. Robb, *J. Phys. Chem. A*, 2004, **108**, 10609.
105 T. A. Miller, in *QuantumDynamics at Conical Intersections*, ed. G. A. Worth and S. C. Althorpe, CCP6, Daresbury, 2004. pp. 25–31, ISBN 0-9545289-1-3.
106 A. Ceulemans, *ChemPhysChem*, 2004, **5**, 1631.
107 M. S. Child, *Adv. Chem. Phys.*, 2002, **124**, 1.
108 T. C. Thompson, D. G. Truhlar and C. A. Mead, *J. Chem. Phys.*, 1985, **82**, 2392.
109 C. A. Mead, *J. Chem. Phys.*, 1983, **78**, 807.